OCTolyzer: Fully automatic analysis toolkit for segmentation and feature extracting in optical coherence tomography (OCT) and scanning laser ophthalmoscopy (SLO) data

Jamie Burke^{1,2,*}, Justin Engelmann^{3,4}, Samuel Gibbon², Charlene Hamid⁵, Diana Moukaddem⁶, Dan Pugh⁷, Tariq Farrah⁷, Niall Strang⁶, Neeraj Dhaun⁷, Tom MacGillivray^{5,9}, Stuart King^{1,†} and Ian J.C. MacCormick^{8,9,†}

Abstract

Purpose To describe OCTolyzer: an open-source toolkit for retinochoroidal analysis in optical coherence tomography (OCT) and scanning laser ophthalmoscopy (SLO) images.

Methods OCTolyzer has two analysis suites, for SLO and OCT images. The former enables anatomical segmentation and feature measurement of the en face retinal vessels. The latter leverages image metadata for retinal layer segmentations and deep learning-based choroid layer segmentation to compute retinochoroidal measurements such as thickness and volume. We introduce OCTolyzer and assess the reproducibility of its OCT analysis suite for choroid analysis.

Results At the population-level, choroid region metrics were highly reproducible (Mean absolute error/Pearson/Spearman correlation for macular volume choroid thickness (CT):6.7 μ m/0.9933/0.9969, macular B-scan CT:11.6 μ m/0.9858/0.9889, peripapillary CT:5.0 μ m/0.9942/0.9940). Macular choroid vascular index (CVI) had good reproducibility (volume CVI:0.0271/0.9669/0.9655, B-scan CVI:0.0130/0.9090/0.9145). At the eye-level, measurement error in regional and vessel metrics were below 5% and 20% of the population's variability, respectively. Major outliers were from poor quality B-scans with thick choroids and invisible choroid-sclera boundary.

Conclusions OCTolyzer is the first open-source pipeline to convert OCT/SLO data into reproducible and clinically meaningful retinochoroidal measurements. OCT processing on a standard laptop CPU takes under 2 seconds for macular or peripapillary B-scans and 85 seconds for volume scans. OCTolyzer can help improve standardisation in the field of OCT/SLO image analysis and is freely available here: https://github.com/jaburke166/OCTolyzer.

Translation relevance Few open-source pipelines provide accurate and reproducible measurements of the retina and choroid from OCT images which are vital to research and clinical practice. OCTolyzer addresses this gap.

Introduction

The retina is a light-sensitive tissue at the back of the eye and is essential for vision, comprising several neural and vascular layers. The inner retinal layers are maintained by the retinal microvascular system sourced by the central retinal artery and vein which branch out from the optic nerve head, while the outer retina (photoreceptors) are sustained by the choroid. This is a dense vascular layer sitting behind the photoreceptors and retinal pigment epithelium, supplied by the short, posterior ciliary arteries ¹.

Optical coherence tomography (OCT) uses low coherence interferometry to collect depth and intensity information from the hyper-reflectivity of retinal tissue. Typically, a confocal, infrared reflectance scanning laser ophthalmoscopy (SLO) image is also acquired and used as a localiser to facilitate clinical interpretation (supplementary Fig. S1). This image shows the en face, superficial retinal vessels along the inner surface of the retina and is very similar to colour fundus photography but with a field of view of 30 degrees (approximately 9 mm²).

OCT is most often used to acquire cross-sectional images of the retina and choroid. The choroid has traditionally received less attention than the retina, since older OCT technology was not very effective at imaging structures posterior to the retinal pigment epithelium. However, recent advances have improved images of the choroid, enabling cross-sectional characterisation

¹School of Mathematics, University of Edinburgh, Edinburgh, UK

²Robert O Curle Ophthalmology Suite, Institute for Regeneration and Repair, University of Edinburgh, UK

³School of Informatics, University of Edinburgh, Edinburgh, UK

⁴Centre for Medical Informatics, University of Edinburgh, Edinburgh, UK

⁵Clinical Research Facility and Imaging, University of Edinburgh, Edinburgh, UK

⁶Department of Vision Sciences, Glasgow Caledonian University, Glasgow, UK

⁷British Heart Foundation Centre for Cardiovascular Science, University of Edinburgh, Edinburgh, UK

⁸Institute for Adaptive and Neural Computation, School of Informatics, University of Edinburgh, Edinburgh, UK

⁹Centre for Clinical Brain Sciences, University of Edinburgh, Edinburgh, UK

^{*}Corresponding and lead author; Email address: Jamie.Burke@ed.ac.uk

[†]Equal contribution

of both the retina and choroid in OCT².

The localiser SLO image of the OCT image-set has also not received much attention, because its role has been mainly to orientate the observer to locations within the cross-sectional image stack. However, the en face SLO has several valuable characteristics: its confocal imaging method produces greater contrast of the vessels, optic disc and fovea over regular colour fundus images³, and the interferometry of the OCT system enables an exact conversion factor from pixel space into physical space, a crucial step in generating clinically meaningful datasets of the retina⁴. In colour fundus systems, comprising a microscope attached to a camera with a flash, heuristic approaches are commonly used to obtain physical measurements, such as optic disc area normalisation⁵.

The OCT/SLO system together capture the retina and choroid and permit a unique assessment of the microvasculature which play a critical role in maintaining eye health. Moreover, there is increasing evidence to suggest that the retinal and choroidal circulations correspond with microvascular changes in structure and function of vital organs like the brain, kidney and heart ^{6,7,8,9}. These observations contribute to the nascent field of "oculomics", the relationship which the ocular system has in the context of systemic health ¹⁰. Moreover, accessibility of OCT systems are improving in terms of cost, size and availability outside of the clinic ^{11,12};13;14, so providing a means of automatic processing for the vast volumes of data collected on a global scale would likely provide a significant benefit to research and clinical communities.

Anatomical annotation of the retina and choroid on OCT/SLO is prohibitively expensive in terms of time, labour and is prone to human error. Therefore, there has been a wealth of research into automatic segmentation methods. The majority have focused on retinal OCT layer segmentation, with more than 60 papers examined in a recent comprehensive review ¹⁵. There has been far less focus on choroid segmentation ^{16;17;18}. Similarly, there have been very few methods for retinal vessel segmentation in SLO ^{19;20;21;22;23}.

Many of these previous methods have not been made available to the research community, or require permission or payment to be used. Moreover, it is rare for computational methods to be released with accompanying code for batch processing and feature measurement ²⁴;25;26;27. There has been increasing demand for easy-to-use, open source toolkits to help promote standardisation of ocular parameters in research ²⁸;29;30;17;18;31 and equip general researchers who may not have any specialist training in image analysis. However, there is a distinct lack of similar pipelines for OCT and SLO imaging modalities.

Accordingly, we have developed a fully automatic analysis toolkit, OCTolyzer, for segmentation and feature measurement of cross-sectional retinal and choroidal OCT images and the accompanying en face SLO image. The benefits of OCTolyzer are:

- It is the first of its kind, providing a fully automated endto-end procedure from raw OCT/SLO data to feature measurement of the retina and choroid.
- It is modular, such that each OCT/SLO analysis suite can be used independently. In particular, the SLO analysis suite, SLOctolyzer³¹, offers a more general-purpose approach to SLO image analysis.
- It uses the latest deep learning algorithms for en face retinal vessel segmentation in SLO images, choroidal layer segmentation in OCT, and leverages image metadata to obtain

- retinal layer segmentations in OCT (if available).
- It supports analysis of three core OCT data types: single/radial macular OCT B-scans, macular OCT volume scans, and optic disc-centred OCT peripapillary B-scans. Thus, OCTolyzer's SLO analysis suite supports analysis of macula- and disc-centred SLO images.
- It can be used for batch processing which is easy to deploy and collates clinical measurements into a single file ready for downstream statistical analysis.

Methods

Fig. 1 describes the core elements of OCTolyzer's analysis pipeline. OCTolyzer contains two analysis suites, for the OCT and the corresponding localiser SLO images. OCTolyzer is freely available on GitHub and can be used without author permissions, specialist training or a technical background. OCTolyzer is freely available here: https://github.com/jaburke166/OCTolyzer.

Data

Segmentation model populations The data used to construct the previously published deep learning segmentation models for the OCT and SLO analysis suites have been described 18;17;31. The majority of this data were from cohorts related to systemic health and normative data. Supplementary Table S1 and Table S2, with supporting text, describe the image and population characteristics for the two deep learning models OCTolyzer uses for OCT choroid segmentation. More details can be found in the original papers which describe the OCT choroid segmentation models 18,17. Supplementary Table S3 describe the image characteristics of the five cohorts used to build the segmentation models for OCTolyzer's SLO analysis suite. Additionally, supplementary Table S4 describe which of the cohorts and how many eyes/images were used in each of the three SLO segmentation models for training and evaluation. More details can be found in the original paper describing OCTolyzer's stand-alone SLO analysis suite, SLOctolyzer³¹. All studies and cohorts adhered to the Declaration of Helsinki, received relevant ethical approval, and informed consent from all subjects was obtained in all cases from the host institution.

Reproducibility populations Three cohorts were used in this analysis, i-Test³², Glasgow Caledonian University Topcon (GCU Topcon)³³ and Diurnal Variation for Chronic Kidney Disease (DVCKD)³². We used all available eyes which had repeated data available (at the point of analysis) from each study (120 eyes from 60 participants from the i-Test study, 33 eyes from 21 participants in the GCU Topcon study and 22 eyes from 22 participants in the DVCKD study). Table 1 describes the core image and population characteristics for these three samples.

Acquisition for i-Test 32 used the spectral domain OCT (SD-OCT) Heidelberg Spectralis Standard and FLEX modules, the latter presenting as a mobile version of the former (Heidelberg Engineering, Heidelberg, Germany). During acquisition, two unregistered macula-centred volume scans for each eye was collected, each scan covering a 30×20 degree (approximately 9×6.6 mm, horizontal \times vertical) field of view. Repeated OCT volume scans were taken immediately (within 1 minute) after one another, with enhanced depth imaging (EDI) mode toggled on and off. For each EDI OCT volume, 31 parallel line-scans were collected, linearly spaced approximately 240 microns apart with an automatic real time (ART) B-scan averaging of 50. For

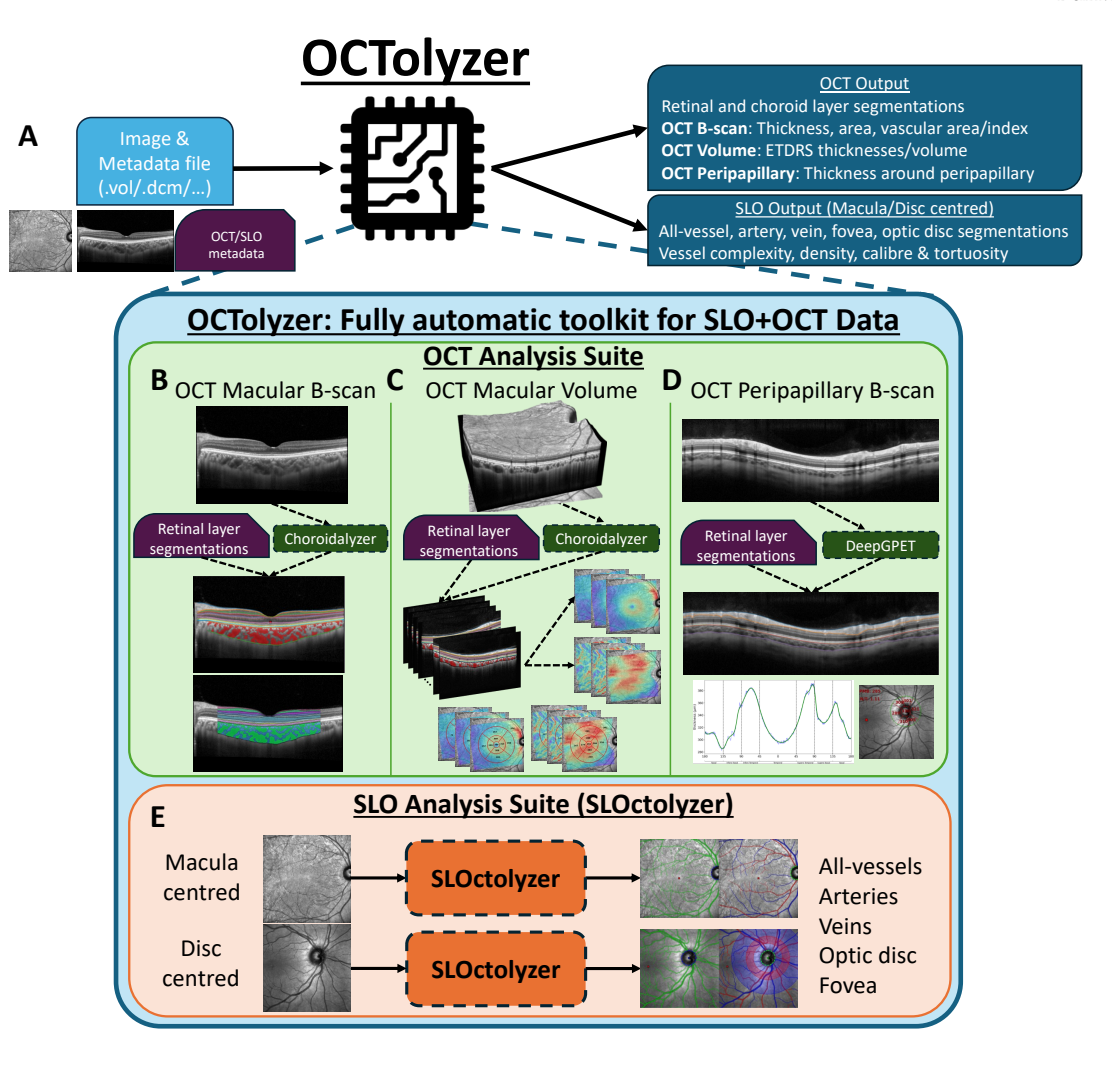


Figure 1 OCTolyzer's pipeline. (A) OCTolyzer expects a file containing the OCT (and optional SLO) image data, and necessary OCT file metadata. (B – E) A deeper dive into OCTolyzer's internal structure. (B – D) OCT analysis suite: analysis pipelines for when OCTolyzer detects a single/radial macular B-scan (B), macular volume scan (C) or peripapillary B-scan (D). (E) SLO analysis suite for macula- or disc-centred SLO localiser images, which accompany OCT capture, using SLOctolyzer 31 .

each non-EDI OCT volume, 61 parallel line-scans were collected, linearly spaced approximately 120 microns apart with an ART of 12. OCT B-scans were of pixel resolution 496 \times 768 (pixel height \times width). Collectively, OCT B-scans comprising the volume scans had an average quality score of 35.58, according to the signal-to-noise ratio index built-in to the Heidelberg scanning device (Heidelberg Engineering, Heidelberg, Germany).

The GCU Topcon study 33 used the swept source OCT (SS-OCT) Topcon DRI Triton Plus device (Topcon, Tokyo, Japan) and collected data for the purposes of assessing diurnal variation of the choroid, primarily targeting hyperopes during recruitment. During CFP+OCT acquisition, a twelve-line, fovea-centred OCT radial scan was captured, starting from a horizontal-line B-scan and rotating clockwise in 30 degree intervals. Repeated scans were taken at the same location during each visit within 5 minutes of each other. OCT B-scans were of resolution 992×1024 and covered approximately 9 mm laterally. Any set of 12 B-scans with an average image quality score less than 88—reported by the signal-to-noise ratio index built-in to the Topcon scanning device (Topcon, Tokyo, Japan) — was excluded. Given repeated acquisition was not the primary aim of the GCU Topcon study,

only 12 participants had repeated OCT data in both eyes and nine participants in one eye.

Participants in the DVCKD study were recruited to assess the impact of time of day on retinochoroidal metrics in healthy volunteers to support research related to chronic kidney disease ³⁴. During acquisition, the SD-OCT Heidelberg Spectralis Standard Module was used to collect horizontal-line OCT Bscans, OCT volume scans and OCT peripapillary scans of the right eye only. While this dataset might be impacted by choroid diurnal variation, it was the only available dataset containing repeated peripapillary B-scans taken on the same day. Thus, only the OCT peripapillary scans were selected to assess OCTolyzer's reproducibility. Peripapillary B-scans collected for the DVCKD study were circular cross-sections of the retina and choroid and centred on the optic disc. B-scans were collected with EDI mode activated using an ART of 100 and had a pixel resolution of 768 \times 1536. The study collected scans at three time points during daylight, in the morning (09:12 \pm 12 minutes), early afternoon (12:36 \pm 7 minutes) and early evening (16:08 \pm 8 minutes).

	Study					
	i-Test ³²	GCU Topcon ³³	DVCKD ^{32;34}			
Cohort demographics						
Participants (Eyes)	60 (120)	21 (33)	22 (22)			
Right eyes (%)	60 (50)	15 (45.5)	22 (100)			
Age (SD)	34.7 (5.2)	23.9 (4.2)	21.3 (2.2)			
Sex, F (%)	60 (100)	9 (43)	10 (45.5)			
Ethnicity	52 White, 6 Asian, 2 Mixed	12 White, 5 Asian, 2 Black, 2 Middle Eastern	Unknown			
Refractive status [†]	3 hyperopes, 31 emmetropes, 26 myopes	9 hyperopes, 8 emmetropes, 3 hyperopes, 1 missing	Axial length 24.1 \pm 1.3 mm — mild myopes.			
Gestation	35.6 ± 3.4	NA	NA			
Study purpose	Pre-eclamptic / normative pregnancy at late gestation	Diurnal variation	Diurnal variation			
Control/Case	45/15	21/0	22/0			
Image characteristics						
Device	Spectralis (Heidelberg)	DRI Triton Plus (Topcon)	Spectralis (Heidelberg)			
OCT Type	Spectral-domain	Swept-source	Spectral-domain			
Scan Pattern	Macular volume	Macular radial	Peripapillary			
Mode	HRA+OCT	CFP+OCT	HRA+OCT			
Time of day (Interval)	All in afternoon (1 minute)	13 morning, 12 afternoon, 8 evening (5 minutes)	Each at 9am, 12:30pm, 4pm (\pm 40 minutes)			
B-scans per eye	31 (EDI) / 61 (non-EDI)	12	1			
ART	50 (EDI) / 12 (non-EDI)	NA	100			
SNR	35.61	>88	>25			
Pixel resolution	496×768	992 × 1024	768×1536			

Table 1 Population demographics and image characteristics of the three samples used for assessing OCTolyzer's reproducibility for choroid analysis. SD, standard deviation; GCU, Glasgow Caledonian university; DVCKD, diurnal variation for chronic kidney disease; HRA, Heidelberg retina angiography; OCT, optical coherence tomography; SLO, confocal infrared reflectance scanning laser ophthalmoscopy; EDI, enhanced depth imaging; ART, automatic real time; SNR, signal-to-noise ratio; CFP, colour fundus photography. † : myopic/hyperopic status defined as <-1/> 1 dioptres. Dioptre measurements for the i-Test sample was the scan focus values collected each OCT scans' metadata, for the GCU Topcon sample this was each eye's spherical equivalent and for the DVCKD sample this data was unavailable, but their axial length was measured.

OCTolyzer's segmentation module

OCTolyzer's OCT and SLO analysis suites each have separate segmentation modules for anatomical segmentation of the choroidal layer and vessels in OCT images and en face retinal vessels, fovea and optic disc in SLO images. The segmentation models have been described previously ^{17;18;31}.

OCT Segmentation OCTolyzer does not have a standalone algorithm for retinal layer segmentation, but supports extraction of the segmented layers from image metadata, as it's common for OCT manufacturers to have their own built-in segmentation tool for the retinal layers. Whether all retinal layers have been quality checked is at the discretion of the end-user. This is typically performed on the manufacturers proprietary software, such as the Heidelberg Eye Explorer (HEYEX) viewer (Heidelberg Engineering, Heidelberg, Germany)³⁵.

Choroid segmentation for macular OCT B-scans is with Choroidalyzer ¹⁷. Choroidalyzer is a deep learning-based tool which automatically segments the choroidal region and vascula-

ture, and also detects the fovea on fovea-centred OCT B-scans.

Choroid segmentation for disc-centred, peripapillary B-scans is with DeepGPET ¹⁸. DeepGPET is a deep learning-based tool which automatically segments the choroidal region and is robust to segmenting peripapillary choroids, of which it was not trained on (supplementary Fig. S2).

SLO Segmentation There are three segmentation models for the SLO analysis suite, one for all-vessel segmentation, one for fovea detection and another for segmentation of the SLO into arteries, veins and the optic disc (artery-vein-optic disc detection)³¹.

OCTolyzer's measurement module

OCTolyzer's OCT analysis suite supports retinochoroidal spatial measurements on OCT scans, while the SLO analysis suite supports measurement of vessel complexity, density, calibre and tortuosity of the en face retinal vessels in SLO images ³¹.

Macular B-scan For macular OCT B-scans, Choroidalyzer automatically detects the fovea pixel coordinate if the scan is fovea-

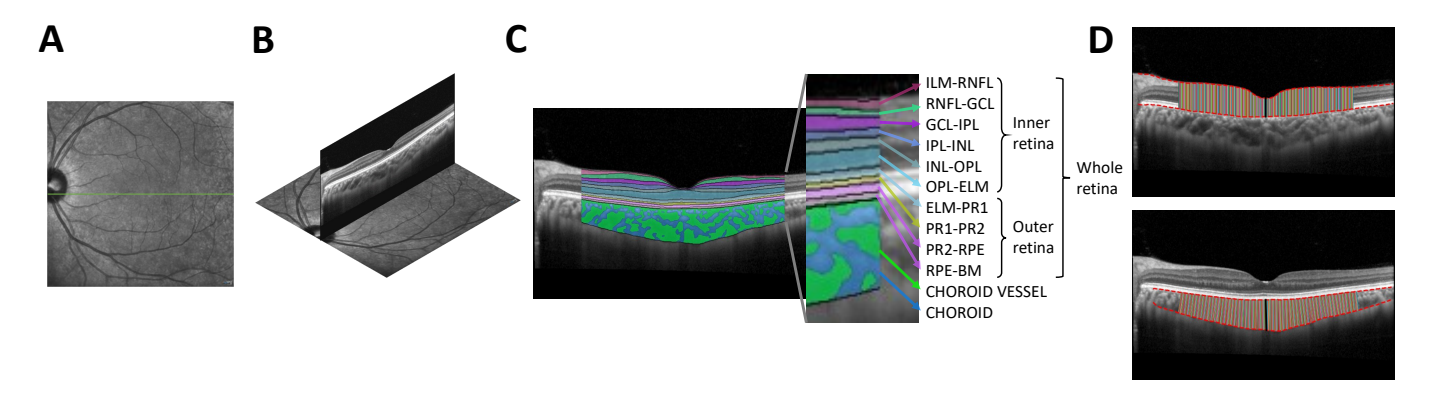


Figure 2 A diagram of how measurements are made for a single macular OCT B-scan. (A) localiser SLO with line of OCT acquisition shown in green. (B) Exemplar horizontal-line OCT B-scan overlaid onto the localiser SLO. (C) OCT B-scan with retinal and choroid layer segmentations and layer names overlaid — retinal layer definitions are presented in supplementary Table S5. (D) Thickness lines drawn between upper and lower boundaries for the whole retina (top) and choroid (bottom) to demonstrate measuring per A-scan and locally perpendicular to upper boundary. The black solid line represents the subfoveal thickness measurement.

centred. For a user-specified, fovea-centred region of interest (RoI), we measure thickness (subfoveal and averaged over the RoI), area for all available layers, and choroidal vessel area and vascular index. Retinal layer segmentations are assumed to be available in the image metadata. Otherwise, retinal measurements are not made.

We define the choroid as the space posterior to hyper-reflective Bruch's complex and anterior to the sclera. To account for choroidal curvature, thickness measurements are made by measuring a straight line micron distance between the upper and lower boundaries, locally perpendicular to the upper boundary. Retinal layer thicknesses by default are measured per A-scan, i.e. through measuring a vertical, straight line micron distance between upper and lower boundaries. Area measurements are the number of pixels within the RoI constituting the layer (or choroid vessel), converted into mm². Choroid vascular index is the ratio of vessel area to total choroid area in the RoI. Fig. 2 shows an exemplar OCT B-scan with the retina and choroid fully segmented (C), with thickness lines overlaid for the retina and choroid separately (D).

Macular volume scan An OCT volume is made up of several, parallel OCT B-scans in sequence. Choroidalyzer is used to segment the choroidal layer and vessels for all B-scans. The foveal pit is assumed to be present in one or more of the OCT B-scans, and the central B-scan in the stack may not necessarily be at the centre of the macula. Thus, the B-scan and corresponding pixel coordinate which has the highest probability outputted from Choroidalyzer's fovea detection is selected as the central B-scan and fovea coordinate, respectively — i.e., at the centre of the macular volume scan. The fovea on the localiser SLO is detected by cross-referencing the fovea detected from the OCT data. Retinal layer segmentations are assumed to be available in the image metadata. Otherwise, retinal measurements are not made.

For each layer of interest, thicknesses are taken at every available A-scan (perpendicularly-aligned for choroidal measurements), measuring the distance between the layers' upper and lower boundaries. This is done for all B-scans of the OCT volume, and they are aligned using the lateral location of the fovea — extrapolated from the central B-scan with the detected fovea.

This creates a coarse map of thickness values across the OCT volume, which are then interpolated, smoothed, padded and rotated to align with the region of interest on the localiser SLO. We apply bi-linear interpolation and Gaussian blur to the coarse map to align the maps' pixel resolution to that of the localiser SLO and smooth any interpolation artefacts. The padding centres the thickness map on the fovea, and the rotation ensures perfect registration with the region of acquisition on the localiser SLO. The angle of rotation is detected by measuring the angle of elevation of the B-scan location on the localiser SLO. Supplementary Fig. S3 shows the pipeline for computing a choroid thickness map.

We centre three concentric circles with 1mm, 3mm and 6mm diameters using the fovea on the localiser SLO and split the 3mm and 6mm circles into four, equally sized quadrants. The quadrants are aligned with the angle of elevation of the OCT volume's region of interest. Average thickness (in microns) and interpolated volumes (in mm³) are measured for these 9 sub-regions, constituting all areas of interest along the early treatment diabetic retinopathy study (ETDRS) grid ³⁶. A final measurement is taken as the average over the entire 6mm, circular RoI. Additional choroid vessel density (in micron²) and vascular index (dimensionless) maps are also measured along the ETDRS grid. Any missing values are approximated using nearest neighbour interpolation, and the percentage of missing values per sub-region are logged and outputted to the end-user.

Fig. 3 shows the core steps in processing an OCT volume, from raw data to measurement.

Peripapillary B-scan For every layer of interest — peripapillary choroid and any available retinal layers from image metadata — we generate a thickness array, measuring a micron distance every A-scan (column pixel). We do not measure locally perpendicularly for the choroid because the sinuous nature of the B-scan is a result of the circular-shaped acquisition line, and not curvature due to poor acquisition or differences in anatomy like with macular B-scans which have a linearly shaped scan pattern. The array is padded with zeros if the segmentation doesn't reach the lateral ends of the image, alerting the end-user of any incomplete segmentations. This is because the thickness array must extend across the entire lateral axis due to the continuity of the

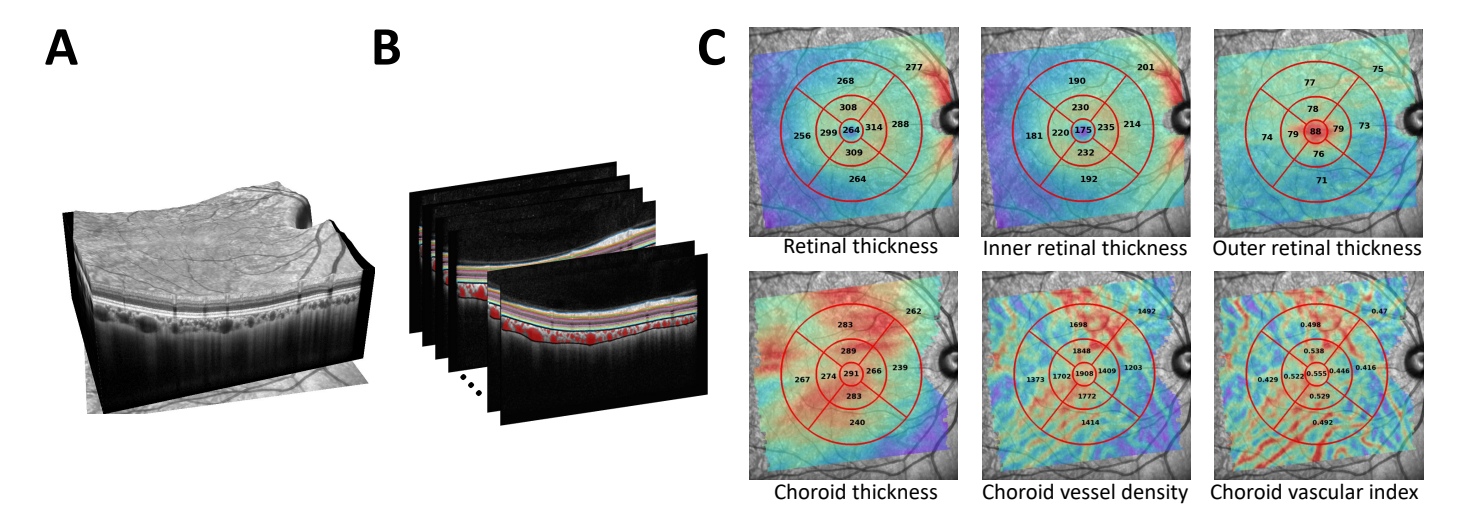


Figure 3 A diagram of how measurements are made for a macular OCT volume. (A) Exemplar 3D visualisation of an OCT volume scan. (B) Sequential B-scans with retinal and choroid layer segmentations overlaid. (C) Thickness maps of the inner, outer and whole retina (top) and choroid thickness, choroid vessel density and choroid vascular index maps (bottom), with average measurements along the ETDRS grid overlaid. All inner retinal layer thickness maps can also be computed and measured.

two ends of the B-scan.

To create the peripapillary grids, we define the centre (0 degrees) of the temporal peripapillary grid (the lateral position along the B-scan) by deducing the point along the circular acquisition region (on the localiser SLO) which is co-linear with the optic disc centre and fovea centre. If the localiser SLO is unavailable, then the centre is taken as the lateral centre of the Bscan. Thus, without the SLO, the peripapillary grid will likely be off-centre. The thickness array can then be divided into temporal (-45 – 45 degrees), supero-temporal (45 – 90 degrees), superonasal (90 – 135 degrees), nasal (135 – -135 degrees), infero-nasal (-135 – -90 degrees) and infero-temporal (-90 – -45 degrees) grids. Average thickness (in microns) is measured per grid, as well as the nasal-to-temporal (N/T) ratio and papillomacular bundle (-30 – 30 degrees). A final average over the whole B-scan is also measured. Thickness profiles for each layer are also generated, showing the raw thickness evolution and a moving average estimate, with the peripapillary grid and angular thresholds overlaid. Fig. 4 shows a series of images describing this procedure.

We have also built in an overlap index to assess how offcentre a peripapillary scan may be from the centre of the optic disc. The overlap index computes the distance between the acquisition's centre and the optic disc centre inferred from the SLO analysis suite, and is measured as a percentage of the optic disc diameter. We have empirically determined a threshold of 15% to likely exceed acceptable centring of the OCT peripapillary scan on the optic disc. See supplementary Fig. S4 for two examples, one of which exceeds the 15% threshold.

localiser SLO The measurements obtained from the en face retinal vessels segmented from the localiser SLO image have been described ³¹. In brief, we have adapted the code provided by Automorph ²⁹ to measure vessel complexity, density, tortuosity and calibre of the arteries, veins and all-vessels from the localiser SLO. We measure fractal dimension (using the Minkowski-Bouligand dimension ³⁷), vessel density (ratio of vessel pixels to pixel resolution), global vessel calibre (ratio of vessel pixels to skeletonised vessel pixels) and local vessel cal-

ibre (vessel calibre computed and averaged across individual vessel segments). We also measure central retinal artery and vein equivalents (CRAE, CRVE), computed using the Knudston approach ³⁸, as well as tortuosity density ³⁹. For both macula- and optic disc-centred SLO images, all measurements are computed across the whole image. For optic disc-centred SLO images, CRAE/CRVE, local vessel calibre and tortuosity measurements are computed for circular regions of interest centred on the optic disc, zones B and C which have standard definitions ⁴⁰.

OCTolyzer's pipeline

Input OCTolyzer fully supports .vol file formats (from Heidelberg Engineering imaging devices) and was designed around such file formats for extracting macular B-scan, volume and peripapillary B-scan data using the EyePy python package ⁴¹. There is currently no support for .e2e files as current python-based file readers ^{41,42} are unable to locate the necessary pixel length scales for converting from pixel space into physical space. Additionally, we have not considered support for other proprietary file formats such as .fda, .fds, .img and .oct, due to the propensity for storing ophthalmic image and metadata in DICOM (.dcm) format for purposes of vendor neutrality. .dcm file formats currently have limited support but we are working on this presently. See supplementary Fig. S5 for information on OCTolyzer's expected input, setup and interface.

OCT analysis suite OCT B-scans are automatically brightened to promote accurate segmentation of the choroidal layer. Gammalevel contrast enhancement is used to brighten OCT B-scans such that their mean pixel intensity is approximately 0.2 and normalised in [0, 1]. This is particularly important for OCT B-scans which show large choroids or where EDI mode was not activated during acquisition.

Choroidal vessels can be corrupted by superficial retinal vessel shadowing, where the OCT beam penetrates through superficial retinal vessels sitting perpendicular to the incident laser light, which consequently darkens the corresponding A-scans of the deeper outer retinal and choroidal structures behind it ⁴³. We apply a multiplicative compensation factor for each A-scan, au-

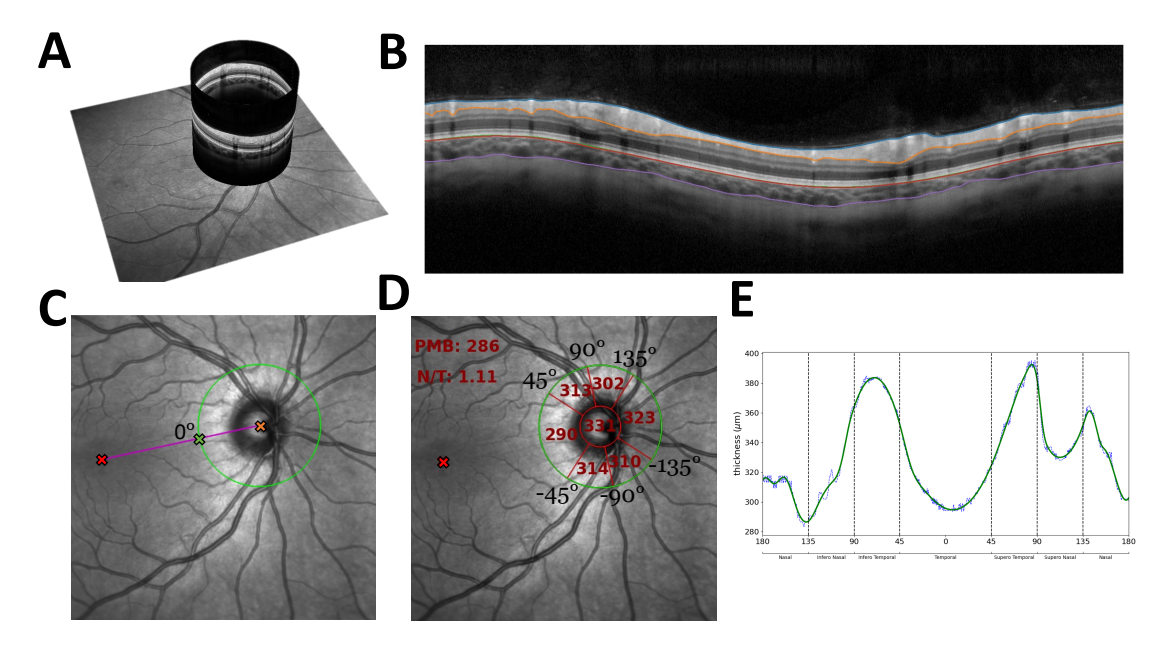


Figure 4 A diagram of how measurements are computed for an OCT peripapillary B-scan. (A) An exemplar OCT peripapillary, circular OCT B-scan overlaid onto the localiser SLO. (B) The circular OCT B-scan with retinal and choroid layer segmentations overlaid. (C) Detection of the centre of the temporal peripapillary grid. (D) Division of the circular OCT B-scan into the 6 peripapillary grids, with output values from measuring the peripapillary retina overlaid. (E) Thickness profile of the peripapillary retina, with peripapillary grid thresholds overlaid.

tomatically brightening the shadow-corrupted pixel columns ⁴⁴. Column-wise compensation factors are computed as the element-wise ratio between each A-scans' averaged signal (axially), and the lateral moving average over these averaged A-scans — the latter signal smooths out any sudden dips in brightness from the shadow-corrupted A-scans.

B-scans are segmented to extract the choroidal layer and vessels using Choroidalyzer or DeepGPET ^{17;18}. For peripapillary B-scans, the image is first padded laterally with 240 pixels by reflecting each opposite edge — as the B-scan is circular and thus continuous at either end — to ensure the entire width of the choroid is segmented. Empirically determined thresholds of 0.5 and 0.25 are used for obtaining binary choroid region segmentation masks using Choroidalyzer and DeepGPET, respectively. It is important for peripapillary choroids to be segmented end-to-end laterally, and given that DeepGPET's training pipeline did not include peripapillary OCT B-scans, a lower threshold was selected to further mitigate under-segmented peripapillary choroids.

Choroidalyzer outputs the raw probability map for choroid vessel segmentation. This is to account for poorly defined vessel walls which are often visualised in OCT B-scans whose cross-section through the choroid cuts across the dense vascular space, resulting in a highly heterogeneous visualisation of choroidal vessels in terms of size and shape.

For fovea detection in macular B-scans, the horizontal and vertical location of the fovea coordinate on the B-scan is detected by passing 21-wide and 51-long triangular filters over the raw probability map outputted from Choroidalyzer ¹⁷.

Any available retinal layer segmentations from image metadata are combined with the choroid layer and vessel segmentations and fed into OCTolyzer's measurement module. The relevant measurements of thickness, area, volume, vascular index and vessel density are computed and saved out. Additionally, key visualisations for assessing segmentation quality are saved out during processing. This includes representative B-scans with segmentations overlaid for single macular and peripapillary B-scans, and macular thickness/density maps with ETDRS grid values overlaid onto the localiser SLO for OCT volume data (if the SLO is available). For peripapillary OCT, thickness profiles and peripapillary grids are saved out. To prevent problems of memory consumption during large-scale batch processing, saving these out are optional.

SLO analysis suite This suite has been described previously ³¹. The segmentation module resizes the SLO images to a common resolution of 768×768 , and the outputted segmentation maps are resized back to input resolution. If macula-centred, the fovea coordinate from the OCT is used to cross-reference the corresponding fovea on the localiser SLO. Segmentation masks are binarized using a threshold of 0.5, and the vessel maps are postprocessed using a series of morphological operations to promote connectivity and remove small false positive regions. The optic disc is modelled as an ellipse for optic disc-centred SLO images, and the diameter of the optic disc is measured as the average of the minor and major axis lengths. The measurement module measures vessel complexity, tortuosity and calibre of all-vessels, arteries and veins for the whole image, and additionally for zones B and C in disc-centred images. Optionally, segmentation maps are saved out, as well as a composite image showing the detected fovea, optic disc, veins and arteries overlaid onto the localiser SLO for assessing segmentation quality. OCTolyzer also supports manual correction of erroneous en face retinal vessel segmentations using ITK-Snap 45. Upon manual annotation, OCTolyzer can be rerun again and the manually annotated segmentations will be used to recompute the en face retinal vessel measurements.

Output OCT layer segmentations, SLO segmentation masks, thickness maps, a process log and summary measurements for the processed OCT/SLO file are saved out. Alongside summary measurements, key metadata extracted from the input file are saved out, such as the exact field of view captured, the angle of elevation of the OCT volume scan during acquisition, the average quality of the OCT data, resolution and pixel lengthscale information. Additionally, we save out useful metadata during processing, including coordinates of the fovea on the B-scan and/or localiser SLO, the centre of the optic disc and it's estimated radius. Supplementary Table S6 presents a full list of the metadata outputted by OCTolyzer after processing a .vol RAW file from a Heidelberg Engineering device. See supplementary Fig. S6 for information on OCTolyzer's outputs.

Statistical analysis

We investigate the reproducibility of OCTolyzer's segmentation models for choroid OCT data on downstream clinical measurements. The reproducibility of the SLO segmentation models has been assessed previously ³¹. We use Choroidalyzer to segment the macular OCT data in the i-Test and GCU Topcon samples, and DeepGPET to segment the peripapillary OCT data in the DVCKD sample.

For the i-Test sample, we measured average choroid thickness and choroidal vascular index in the 9 ETDRS grid values per eye for each repeated pair. Thus, there were 1080 comparisons made for this sample. For the DVCKD sample, we measured average choroid thickness in the 6 peripapillary grids, and the papillomacular bundle for each eye. Note, there are three images per eye so we compare pairwise, chronological measurements (morning – afternoon, afternoon – evening) so that there were 308 comparisons made. As we are comparing measurements across the day, diurnal variation of the choroid is a potential confounding factor for this sample. Thus, we address the longitudinal evolution of the peripapillary choroid too.

For each participant in the GCU Topcon sample, OCT B-scan capture was collected throughout the day, with some examinations containing repeated acquisitions. There were 79 instances of repeated OCT B-scan data overall, and approximately 25% of these including more than two acquisitions per examination. Additionally, each acquisition included 12 OCT B-scans per eye. To prevent any sampling bias and remain objective in our reproducibility analysis, we selected one repeated pair per eye to maximise equal sample size for morning, afternoon and evening acquisition where possible. This led to selecting 13 repeated pairs from the morning, 12 from the afternoon and 8 from the evening. Thus, there were 396 comparisons made from 33 eyes, using subfoveal choroidal thickness, choroidal area and choroid vascular index in a 6mm, fovea-centred region of interest.

We measure the reproducibility of Choroidalyzer and Deep-GPET at the population-level, reporting population mean and standard deviation, as well as mean absolute error (MAE) and Pearson, Spearman and intra-class correlation (ICC(3,1)) coefficients. Additionally, we show correlation plots and use Bland-Altman ⁴⁶ plots to assess the relationship between repeated measurements and the distribution of residuals.

We also report the reproducibility of Choroidalyzer and Deep-GPET at the eye-level, using a novel estimate of measurement noise λ^{47} . For each feature, λ measures the within-eye variability in units of between-eye variability and is calculated as the ratio between the standard deviation of within-eye measurements and the standard deviation of between-eye measurements.

Within-eye and between-eye standard deviations are measured by averaging the measurements for each repetition in an eye's pair, and taking the standard deviation for each pair and across pairs, respectively. Thus, since we report 9 values per ETDRS grid for the OCT volume comparison, we take an average of these 9 values for each member of the repeated pair, thus creating a single, representative pair of measurements per eye. We do a similar averaging for the measurements in both the GCU Topcon and DVCKD samples.

Finally, we measured the execution time of OCTolyzer's OCT analysis suite and entire pipeline for each OCT data type which it supports. We deployed OCTolyzer with and without the SLO analysis suite to analyse each exemplar OCT data type 100 times and reported mean and standard deviation execution time in seconds. Repeated experiments were run on a standard, Windows laptop with a 4 year old i5 CPU with 16GB of RAM, but no GPU.

Results

Reproducibility

Population-level Table 2 presents the reproducibility performance of OCTolyzer's OCT analysis suite for all three OCT data types which it supports. OCTolyzer's analysis suite for choroid region segmentations had excellent correlations across all three cohorts using Choroidalyzer and DeepGPET (Pearson/Spearman for ETDRS choroid thickness (CT): 0.9933/0.9969, B-scan subfoveal CT (SFCT): 0.9858/0.9889, B-scan choroid area (CA): 0.9835/0.9870, peripapillary CT: 0.9942/0.9940). Reproducibility for choroid vascular index (CVI) was slightly lower but still good (ETDRS CVI: 0.9669/0.9655, B-scan CVI: 0.9090/0.9145).

Measurements taken in the GCU Topcon suggested these individuals had much thicker subfoveal choroids (mean \pm SD of 386.9 \pm 110.9 μm), compared to the i-Test measurements (mean \pm SD of 275.7 \pm 91.8 μm). While the i-Test sample was older than the GCU Topcon sample, the GCU Topcon study did target hyeropes during recruitment, thus resulting in smaller eyes and thicker choroids. Moreover, the i-Test sample represent ETDRS grid measurements which are taken as averages over macular sub-regions, allowing for noise in measurement error to be averaged out unlike point-source subfoveal choroid thickness measurements (SFCT). The peripapillary choroids were thinnest in the DVCKD sample (mean \pm SD of 169.9 \pm 54.1 μm), which makes sense given peripapillary choroids, nearer the disc, are thinner than macular choroids.

These observations explain why we see higher mean absolute error (MAE) in the GCU Topcon cohort (MAE: $11.6~\mu m$) compared with the peripapillary (MAE: $5.0~\mu m$) and volume data (MAE: $6.7~\mu m$). Additionally, this also highlights the importance of reporting values over an area through averaging, rather than taking a single point-source measurement. Nevertheless, these errors are still below any change expected due to diurnal variation $^{48;49;50;51;52}$, which changes by approximately $30~\mu m$ over the course of the day. These errors are also below the threshold expected to exceed manual rater agreement in SFCT 53 , which has been reported as a mean inter-rater error of $32~\mu m$ and intra-rater error of $23~\mu m$.

For CVI, the MAE in the i-Test sample was double that in the GCU Topcon sample. The MAE was worse in the i-Test sample because of the additional speckle noise appearing in each non-EDI member of the i-Test ETDRS comparison, which can make vessel wall boundaries ambiguous. Regardless, these reported

Method	Metric [unit]	Mean (SD)	MAE	Pearson	Spearman	ICC(3,1)
Choroidalyzer						
i-Test	CT [μm]	274.09 (91.80)	6.7342	0.9933	0.9969	0.9962
	CVI	0.51 (0.03)	0.0271	0.9669	0.9655	0.9813
GCU Topcon	SFCT [µm]	392.63 (110.94)	11.5535	0.9858	0.9889	0.9929
	CA [mm ²]	1.62 (0.46)	0.0509	0.9835	0.9870	0.9916
	CVI	0.53 (0.03)	0.0130	0.9090	0.9145	0.9522
DeepGPET						
DVCKD	CT [μm]	169.60 (54.07)	5.0320	0.9942	0.9940	0.9971

Table 2 Reproducibility performance for OCTolyzer's OCT analysis suite using Choroidalyzer and DeepGPET. All Pearson and Spearman correlations were statistically significant with P-values P < 0.0001. SD, standard deviation; GCU, Glasgow Caledonian university; DVCKD, diurnal variation for chronic kidney disease; MAE, mean absolute error; ICC, intra-class correlation; SFCT, subfoveal choroid thickness; CT, choroid thickness; CVI, choroid vascular index; CA, choroid area.

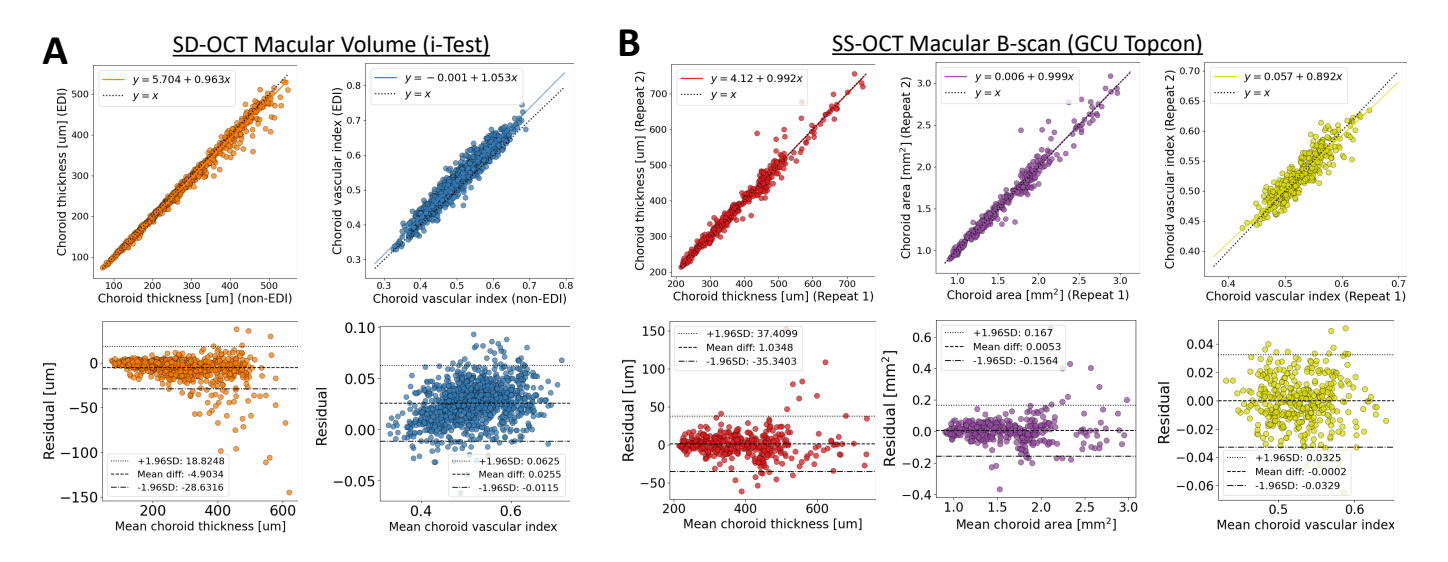


Figure 5 Correlation and Bland-Altman plots for assessing the reproducibility of OCTolyzer's analysis suite for macular OCT data using Choroidalyzer¹⁷. (A) Reproducibility for SD-OCT macular volume scans with EDI mode toggled on and off from the i-Test sample. (B) Reproducibility of SS-OCT macular B-scan pairs from the GCU Topcon sample.

errors are five times below recently reported repeatability of CVI across macular OCT volumes from different manufacturers ⁵⁴. Ma, et al. ⁵⁴ presented a mean difference between SD-OCT and SS-OCT of 0.13, while here we present a MAE of 0.0271 for ETDRS CVI (comparing SD-OCT macular volume data between EDI and non-EDI acquisition), and 0.0130 for B-scan CVI for repeated SS-OCT B-scans.

Fig. 5 show the correlation and Bland-Altman plots for the SD-OCT i-Test and SS-OCT GCU Topcon macular OCT samples. Generally we see that for larger choroids there is larger error in regional metrics. In the case for i-Test, this is entirely expected because the optical signal for non-EDI OCT acquisition degrades the deeper through the eye it penetrates, and the visibility of the deeper choroidal vasculature decays rapidly also. This is also the case for larger choroids in general, and thus why we see similarly larger error in the GCU Topcon sample — the largest choroid had a SFCT of 756 μm (approximately 3.25 standard deviations away from the mean).

The distributions in the Bland-Altman plots for SD-OCT mac-

ular OCT volume data in Fig. 5 show under-prediction of CT and over-prediction of CVI for the non-EDI scans of each pair, while the distributions for macular SS-OCT B-scan data are perfectly centred. The under-prediction of CT in the non-EDI measurements was likely because of the aforementioned optical signal decay in non-EDI scans, which had a direct consequence on CVI, as the vascular index is normalised by the size of the choroid, leading to over-prediction of CVI in non-EDI measurements. However, this under-/over-prediction is unlikely to be clinically significant.

Fig. 6(A) show the correlation and Bland-Altman plots for comparing pairwise peripapillary grid CT measurements for morning vs. afternoon and afternoon vs. evening (with scatter points coloured accordingly). The first striking observation is the degree of separation measurements have between pairwise time point comparisons. The residuals of measurements comparing afternoon and evening are centred around 0, while residuals comparing morning and afternoon appear to be almost consistently below the residual origin (and identity line in the

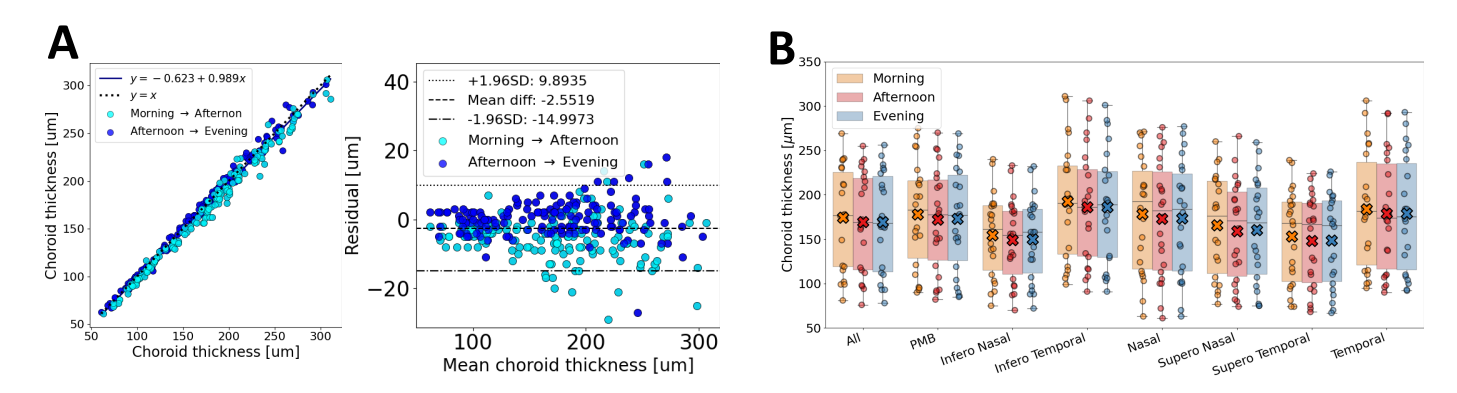


Figure 6 (A) Correlation and Bland-Altman plot for all chronologically paired (morning – afternoon and afternoon – evening) choroid thickness measurements in all peripapillary grids. (B) Longitudinal evolution of average choroidal thickness in each peripapillary grid shown as box-plots, with mean values overlaid as crosses.

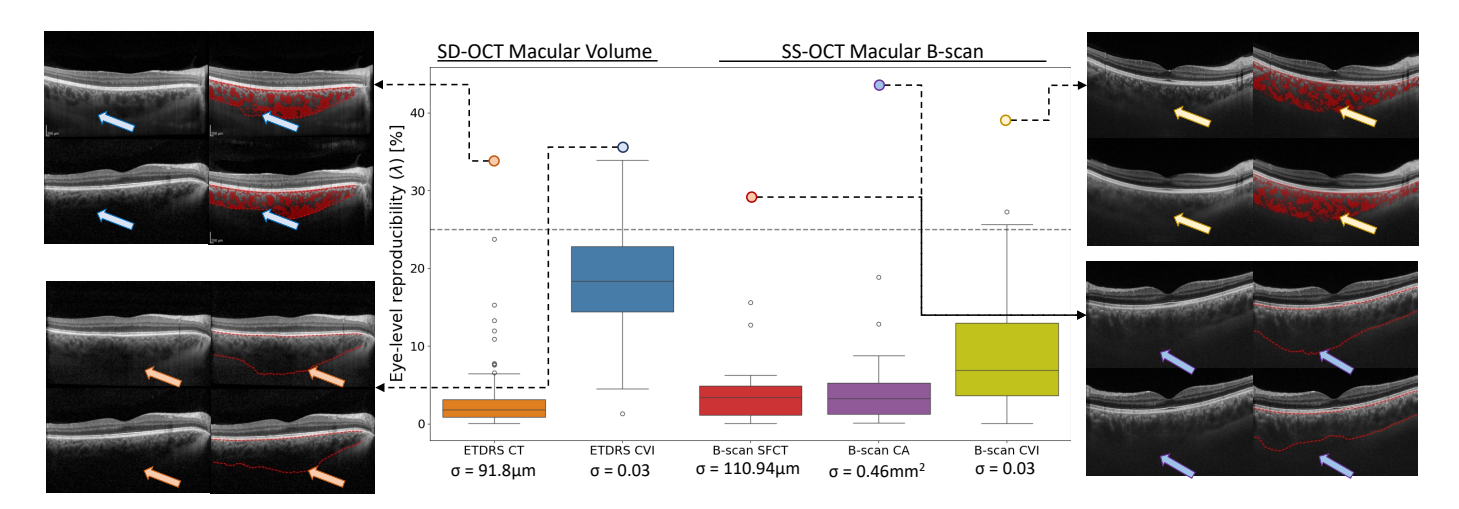


Figure 7 Reproducibility of OCTolyzer's OCT analysis for macular OCT data using Choroidalyzer¹⁷ at the eye-level. We show distributions of eye-level measurement noise λ for both the i-Test macular SD-OCT volume data and GCU Topcon macular SS-OCT B-scan data. Representative B-scans, with segmentations overlaid in red, are selected and shown for the major outliers with arrows indicating the source of the error. The between-eye standard deviations are shown below each box-plot.

correlation plot).

Fig. 6(B) shows the longitudinal evolution of peripapillary choroid thickness for each peripapillary grid between morning, afternoon and evening, with the mean value per time point and grid shown as coloured crosses. Across the board, morning measurements appear larger than afternoon and evening. This corresponds to the trend observed in measuring the same choroids manually in the macula ³⁴ (shown in their supplementary materials), as well as the natural diurnal variation of the choroid observed in other studies ⁴⁸;49;50;51;52</sup>. These previous studies have reported choroidal fluctuations over the course of day with an amplitude of approximately 30 μ m, and the majority reporting larger CT measurements in the morning, compared to the afternoon and evening.

Thus, given that the largest residuals were those observed between morning and afternoon, and that we know the choroid thins between this time period, we propose that the diurnal variation of the choroid is the primary driver of the largest residuals in measuring peripapillary choroid thickness with OCTolyzer, and not segmentation error.

Individual-level Fig. 7 and Fig. 8 presents the reproducibility of OCTolyzer's OCT analysis suite for the macular and peripapillary OCT data at the eye-level, respectively. We present box plots to describe the distribution of measurement noise λ , expressed in terms of the overall population variability (shown below the box-plots as the value σ).

For choroid region metrics, OCTolyzer's eye-level measurement noise was very low compared to the populations natural variability, with the upper quartile of the box-plot distributions for ETDRS CT/B-scan SFCT/B-scan CA sitting below 5% of each features population standard deviation, and below 10% for peripapillary CT. In the latter case, the eye-level variability is confounded with natural diurnal variation of the choroid, and the population standard deviation for the DVCKD sample was about half of the values for the i-Test and GCU Topcon samples. Thus, for choroid region metrics, segmentation error contributes to only 5-10% of the overall population variability.

We observed higher variability in the choroid vessel metrics at the eye-level, with B-scan CVI measurement noise primarily sitting below 15% of the population standard deviation (σ =0.03) and 25% for ETDRS CVI (σ =0.03). This suggests that

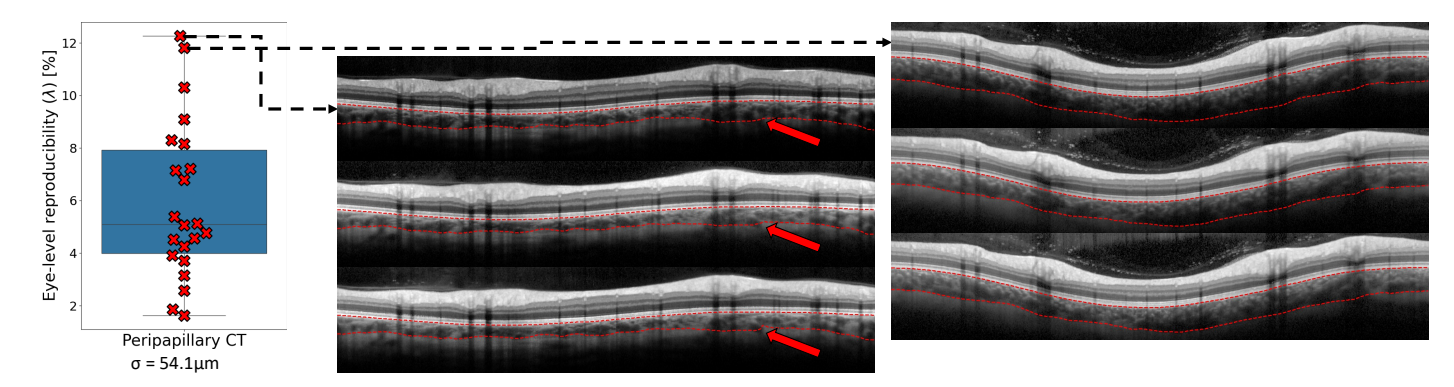


Figure 8 Reproducibility of OCTolyzer's OCT analysis suite for OCT peripapillary data using DeepGPET ¹⁸ at the eye-level. We show the distribution of the eye-level measurement noise λ for peripapillary CT in blue, and the red crosses are the individual values for λ . The peripapillary OCT B-scans of the two major outliers are shown to the right for all three time points, with choroid layer segmentations overlaid in dashed red. The red arrows show the only obvious, but minimal, difference in segmentation.

B-scan type	OCT resolution	SLO resolution	Choroid segmentation	OCT analysis suite	OCT+SLO analysis suite
Macular OCT B-scan	$1\times496\times768$	768×768	0.31 (0.02)	1.55 (0.13)	22.40 (0.97)
Macular OCT volume	$61\times496\times768$	768×768	16.8 (1.60)	85.00 (3.65)	109.00 (3.11)
Peripapillary OCT B-scan	$1\times768\times1536$	1536×1536	1.56 (0.23)	2.29 (0.14)	128.00 (6.37)

Table 3 Average (standard deviation) execution time in seconds of the OCT analysis suite (always performed by default) and the combined execution time for both OCT and SLO analysis suites.

the CVI measurements are less reliable than the regional metrics, and more so for ETDRS CVI. However, ETDRS CVI could have higher variability than B-scan CVI because of the image quality difference between EDI and non-EDI volume pairs (ART 50 for EDI volume data compared to ART 12 for non-EDI volume data), as well as the unregistered nature of the volume scans which have different B-scan sampling rates (31 B-scans per EDI volume compared 61 B-scans per non-EDI volume) and slightly different regions of interest up to some rotation — leading to a different stack of cross-sections of the dense, heterogeneous choroidal vasculature — being captured.

The major outliers for the macular OCT B-scans shown in Fig. 7 are mainly thick choroids whose lower boundaries (arrows) have poor visibility primarily due to decaying optical signal. This has a direct consequence for the CVI outliers, as CVI is normalised by the estimated size of the choroid. Moreover, image quality plays a clear role in poor quality segmentation, such as for the major outlier for B-scan CVI, where one of the repeated pair has poorer contrast and thus poor vessel wall definition. It is encouraging to see that major outliers are coming from challenging cases of thicker choroids with obscure choroid-scleral junctions and poor quality vessel wall definition.

In Fig. 8, we show the B-scans of the major outliers at each time point with the segmentations overlaid using DeepGPET 18 . Any differences (red arrows) are minimal, and the segmentations do not look qualitatively different. These two cases were the major outliers due to the difference in CT observed from morning – afternoon (a negative differential of 15 and 14 μ m in average CT, respectively) relative to their afternoon – evening change (a positive differential of 1 and 2 μ m, respectively). Thus, we propose the major outliers are primarily driven by minimal diurnal variation of the choroid, and not segmentation error.

Execution time

Using a standard laptop CPU, OCTolyzer was able to fully process a single line OCT B-scan in 1.55 \pm 0.1s (pixel resolution 496 \times 768). An OCT volume with thickness maps computed and measured for every retinal and choroidal layer takes 85 \pm 3.7s (pixel resolution 61 \times 496 \times 768). Execution time would improve if the choroid was measured per A-scan (64 \pm 2.5s), rather than locally perpendicular to its upper boundary, and significantly so with GPU acceleration.

An OCT peripapillary scan can be fully processed in 2.29 \pm 0.14s (pixel resolution 768 \times 1536), and takes 1.56 \pm 0.2s to segment the choroidal layer. To align the peripapillary grid, the localiser must be available (as an SLO image) and the fovea and optic disc must be segmented, which increases execution time to 30.70 \pm 2.10.

Execution time increases when the SLO analysis suite is toggled on, particularly for disc-centred SLO images (OCT peripapillary scans), because there are three regions of interest measured for each vessel type (all-vessel, artery, veins). However, this is still acceptable performance on a standard laptop CPU, suggesting its feasibility to be used for large scale OCT/SLO image analysis.

Discussion

We have developed a fully automatic method, OCTolyzer, for segmentation and feature extracting in OCT and SLO data. While the reproducibility of OCTolyzer's SLO analysis suite (SLOctolyzer) has been assessed previously ³¹, OCTolyzer's OCT analysis suite also demonstrates excellent reproducibility across the three different OCT data types of which it supports, both at the population- and eye-level.

Across macular OCT B-scans, macular OCT volume scans and peripapillary OCT B-scans, OCTolyzer had very high corre-

lations across repeated measurements (Pearson, Spearman and intra-class correlations for regional metrics were all greater than 0.98, and 0.91 for choroid vascular index in the macular data). Mean absolute errors from all paired samples in the repeated macular OCT data were below the values of previously reported agreement thresholds 53,54 .

The systematic bias observed in the macular OCT volume data was a result of comparing repeated scans where EDI mode was toggled on and off, increasing the potential for the non-EDI scan of each pair having poor choroid-scleral junction visibility. The residuals for vessel metrics (CVI) were well balanced and appeared to show no apparent trend. Major outliers from eyelevel reproducibility analysis for both regional and vessel metrics in macular OCT data highlighted the challenge larger choroids pose for segmentation, given the propensity for optical signal degradation.

Nevertheless, the majority of measurement error of regional metrics observed for macular OCT B-scan data were within 5% of the population's natural variability for regional metrics, and 25% for volumetric CVI and 15% for B-scan CVI. However, the population variability is notably smaller for CVI measurements, and the image quality, sampling rate and unregistered nature of the EDI and non-EDI volume pairs all likely played a role in producing greater variability in volumetric CVI. Thus, the macular regional metrics were more reliable than vessel metrics, but they were both still reasonable for the homogeneous (young and healthy) cohorts analysed.

For peripapillary OCT B-scans, the reproducibility results were confounded by natural diurnal variation of the choroid. Analysis of residuals suggested that the major outliers were sourced primarily between morning – afternoon comparisons, rather than afternoon – evening comparisons, and major outliers at the eye-level showed no qualitative difference in segmentation error. Manual measurements of fovea-centred choroidal thickness showed the same longitudinal trend ³⁴ (shown in their supplementary materials), as well as a wealth of literature suggesting choroidal thinning throughout daytime, and specifically between the morning and afternoon ^{48;49;50;51;52}. Thus, this suggests the error observed was primarily driven by diurnal variation and not segmentation error.

OCTolyzer's OCT analysis suite is equipped with choroid segmentation methods which can produce reproducible and clinically meaningful features of the choroid in the macula and around the optic disc. The reproducibility analysis (both at the population- and eye-level) also helpfully provide approximate thresholds which end-users can use to understand whether the change they are observing in the choroid after application of OCTolyzer is due to actual biological change or due to segmentation error.

OCTolyzer's runtime is entirely reasonable for large-scale ophthalmic image analysis, even on a standard laptop CPU, taking 1.55s for a single 496 \times 768 B-scan, 2.29s for a single 496 \times 1536 peripapillary B-scan, and 85s for a 61 \times 496 \times 768 OCT volume scan. AlzEye is a recently collected, large-scale dataset of retinal images from the Moorefield's Eye Hospital NHS Foundation Trust 55 . AlzEye contains 1,567,358 OCT images from 154,830 patients. Assuming the 1,567,358 images were from approximately 25,695 61-stack OCT volume scans, these could be fully processed in approximately 25 days on the same laptop CPU — an upper bound which could be significantly improved upon with GPU acceleration and a stronger CPU.

While OCTolyzer does not have an automatic process for

checking image quality, we are able to inform the user of the signal-to-noise ratio of the OCT B-scan data and use the overlap index to assess how off-centre a peripapillary scan is from the optic disc centre. While OCTolyzer does not have an automatic approach to check segmentation quality, OCTolyzer optionally saves out images of the OCT and SLO images with segmentations overlaid, allowing the end-user to inspect segmentation quality in real-time, and also supports manual annotation of the en face retinal vessels on the localiser SLO — currently OCT segmentations cannot be manually edited. We also alert the enduser in the process log of any obvious segmentation issues. For example, we flag to the end-user where peripapillary choroids have not been segmented end-to-end and pad the missing thickness values with zeros. Additionally, for macular OCT volume scans, if the thickness maps have any missing data within the ETDRS grid this is also flagged and the corresponding missing values are imputed using nearest neighbour interpolation.

There were some limitations associated with our reproducibility analysis of the OCT analysis suite. For example, our paired macular OCT volume data were not registered between acquisitions. Thus, the i-Test sample does not provide a perfect comparison to which segmentation could be the direct cause of measurement error. Similarly for the DVCKD sample, the measurement error observed in the peripapillary choroids of these OCT B-scans were confounded by diurnal variation of the choroid. While we could mitigate for this in the GCU Topcon sample by selecting only one time point, this was not the case for the DVCKD sample. Thus, biological change also contributed to the measurement error we observed in the DVCKD sample.

Moreover, it is important for the reader to be aware of potential data leakage in our reproducibility analysis of the macular OCT data. We use Choroidalyzer to segment macular OCT data on the i-Test and GCU Topcon sample, but these reproducibility samples had a distinct overlap with the dataset used to train or evaluate Choroidalyzer 17 (using ground truth labels previously segmented by DeepGPET 18). Just over a third of the i-Test sample (21 / 60) were used for training or evaluation. However, only the EDI counterpart of their OCT volume pair were used. Thus, while Choroidalyzer had potentially seen 42 eyes (of 120 used for analysis) during model construction to some extent, the image artefacts introduced by deactivating EDI mode still posed a significant challenge to Choroidalyzer's reliability as a method. For the GCU Topcon sample, all eyes featured in at least one or more B-scans for training or evaluation of Choroidalyzer, and a third (11 / 33) of repeated pairs were used for training or evaluation, since many of the B-scans from the hyperopes were excluded from training because DeepGPET failed to segment their thicker choroids 17

There are also some limitations associated with OCTolyzer as a pipeline. Firstly, the pipeline was initially designed for inputting .vol RAW files exported from the HEYEX viewer (and imported into Python using EyePy 41). This proprietary file typically almost always contains the paired localiser SLO image, which is not always the case for other file types (e.g., .dcm files). Therefore, we are working on supporting standalone OCT analysis through .dcm files, i.e., where proprietary files only contain the OCT image data, and potentially excludes automatic retinal layer segmentations.

Additionally, the pipeline does not support automatic retinal layer segmentation other than those accessible from the image metadata. Therefore, manual quality inspection of the segmentations on the device before data extraction and processing with

OCTolyzer is required. Finally, our choroid segmentation methods were built using OCT data related to systemic health change, and not related to eye pathology. Thus, acquiring examples of extreme choroid thinning/thickening due to, say pathological myopathy/polypoidal choroidal vasculopathy would be ideal to assess the robustness of OCTolyzer's OCT choroid segmentation methods to eye pathology.

There are several avenues of future work to extend OCTolyzer as a helpful tool for the general researcher and clinician. As with any large-scale image analysis pipeline, the ability to reject images based on quality or segmentation accuracy is crucial for forming a meaningful dataset of clinical measurements. Current signal-to-noise ratios built into imaging devices do not characterise the quality of the image in the context to which it will be analysed for. Such context-dependent image quality methods are essential in large-scale ophthalmic image analysis.

localiser en face images for OCT acquisition need not necessarily be an SLO image, but sometimes a colour fundus image (or other en face scans like blue-light fundus auto-fluorescence). Currently, OCTolyzer only supports segmentation and feature measurement of the SLO, so providing support for other en face modalities would be ideal.

Conclusion

OCTolyzer is the first open-source, fully automatic analysis toolkit for the retinal and choroidal microvasculature as seen in OCT/SLO data, complete with segmentation and feature measurement of macular OCT B-scans, macular OCT volumes and optic disc OCT peripapillary scans, as well as their corresponding localiser SLO image. OCTolyzer is capable of converting proprietary OCT/SLO data into clinically meaningful and reproducible features of the en face retinal vasculature, cross-sectional retinal layers, choroidal layer and vasculature.

OCTolyzer can be freely downloaded and used without specialist training or proprietary software to run the pipeline. Ultimately, we hope OCTolyzer will help standardise the reporting of ocular measurements, enable large-scale ophthalmic image analysis among the research community, and become a foundational pipeline which the wider research community may continue to extend on and improve, thus addressing the distinct lack of such available pipelines for OCT data.

Acknowledgements

J.B. was supported by the Medical Research Council (grant MR/N013166/1) as part of the Doctoral Training Programme in Precision Medicine at the Usher Institute, University of Edinburgh. For the purpose of open access, the authors have applied a creative commons attribution (CC BY) licence to any author accepted manuscript version arising.

Conflicts of Interest

The authors declare no conflicts of interest.

References

- [1] Sohan Singh Hayreh and Shelagh Bell Hayreh. Uveal vascular bed in health and disease: uveal vascular bed anatomy. paper 1 of 2. *Eye*, 37(13):2590–2616, 2023.
- [2] Richard F Spaide, Hideki Koizumi, and Maria C Pozonni. Enhanced depth imaging spectral-domain optical coherence tomography. *American journal of ophthalmology*, 146(4):496–500, 2008.

- [3] Creig S Hoyt and David Taylor. Pediatric Ophthalmology and Strabismus, Expert Consult-Online and Print, 4: Pediatric Ophthalmology and Strabismus. Elsevier Health Sciences, 2012
- [4] Silke Aumann, Sabine Donner, Jörg Fischer, and Frank Müller. Optical coherence tomography (oct): principle and technical realization. *High resolution imaging in microscopy and ophthalmology: new frontiers in biomedical optics*, pages 59–85, 2019.
- [5] Carolin Schanner, Nina Hautala, Franziska G Rauscher, and Aura Falck. The impact of the image conversion factor and image centration on retinal vessel geometric characteristics. *Frontiers in Medicine*, 10:1112652, 2023.
- [6] Anita Kundu, Justin P Ma, Cason B Robbins, Praruj Pant, Vithiya Gunasan, Rupesh Agrawal, Sandra Stinnett, Burton L Scott, Kathryn PL Moore, Sharon Fekrat, et al. Longitudinal analysis of retinal microvascular and choroidal imaging parameters in parkinson's disease compared with controls. Ophthalmology Science, page 100393, 2023.
- [7] Jamie Burke, Neeraj Dhaun, Baljean Dhillon, Kyle J Wilson, Nicholas AV Beare, and Ian JC MacCormick. The retinal contribution to the kidney–brain axis in severe malaria. *Trends in parasitology*, 2023.
- [8] Craig Balmforth, Job JMH van Bragt, Titia Ruijs, James R Cameron, Robert Kimmitt, Rebecca Moorhouse, Alicja Czopek, May Khei Hu, Peter J Gallacher, James W Dear, et al. Chorioretinal thinning in chronic kidney disease links to inflammation and endothelial dysfunction. JCI insight, 1(20), 2016.
- [9] Ehsan Khalilipur, Zahra Mahdizad, Negin Molazadeh, Hooshang Faghihi, Nasim Naderi, Mohammadreza Mehrabi Bahar, Ata Firouzi, Parham Sadeghipour, Majid Maleki, Sahel Soltani Shahgoli, et al. Microvascular and structural analysis of the retina and choroid in heart failure patients with reduced ejection fraction. *Scientific Reports*, 13(1):5467, 2023.
- [10] Siegfried K Wagner, Dun Jack Fu, Livia Faes, Xiaoxuan Liu, Josef Huemer, Hagar Khalid, Daniel Ferraz, Edward Korot, Christopher Kelly, Konstantinos Balaskas, et al. Insights into systemic disease through retinal imaging-based oculomics. *Translational vision science & technology*, 9(2):6–6, 2020.
- [11] Angelica Ly, Lisa Nivison-Smith, Barbara Zangerl, Nagi Assaad, and Michael Kalloniatis. Self-reported optometric practise patterns in age-related macular degeneration. *Clinical and Experimental Optometry*, 100(6):718–728, 2017.
- [12] Anish Jindal, Irene Ctori, Bruno Fidalgo, Priya Dabasia, Konstantinos Balaskas, and John G Lawrenson. Impact of optical coherence tomography on diagnostic decisionmaking by uk community optometrists: a clinical vignette study. Ophthalmic and Physiological Optics, 39(3):205–215, 2019.
- [13] Reena Chopra, Siegfried K Wagner, and Pearse A Keane. Optical coherence tomography in the 2020s—outside the eye clinic. *Eye*, 35(1):236–243, 2021.
- [14] Ge Song, Evan T Jelly, Kengyeh K Chu, Wesley Y Kendall, and Adam Wax. A review of low-cost and portable optical coherence tomography. *Progress in Biomedical Engineering*, 3(3):032002, 2021.
- [15] Ignacio A Viedma, David Alonso-Caneiro, Scott A Read, and Michael J Collins. Deep learning in retinal optical coherence tomography (oct): A comprehensive survey. *Neu-*

- rocomputing, 507:247-264, 2022.
- [16] Reza Alizadeh Eghtedar, Mahdad Esmaeili, Alireza Peyman, Mohammadreza Akhlaghi, and Seyed Hossein Rasta. An update on choroidal layer segmentation methods in optical coherence tomography images: a review. *Journal of Biomedical Physics & Engineering*, 12(1):1, 2022.
- [17] Justin Engelmann, Jamie Burke, Charlene Hamid, Megan Reid-Schachter, Dan Pugh, Neeraj Dhaun, Diana Moukaddem, Lyle Gray, Niall Strang, Paul McGraw, Amos Storkey, Paul J. Steptoe, Stuart King, Tom MacGillivray, Miguel O. Bernabeu, and Ian J. C. MacCormick. Choroidalyzer: An Open-Source, End-to-End Pipeline for Choroidal Analysis in Optical Coherence Tomography. *Investigative Ophthalmol*ogy & Visual Science, 65(6):6–6, 06 2024.
- [18] Jamie Burke, Justin Engelmann, Charlene Hamid, Megan Reid-Schachter, Tom Pearson, Dan Pugh, Neeraj Dhaun, Amos Storkey, Stuart King, Tom J MacGillivray, et al. An open-source deep learning algorithm for efficient and fully automatic analysis of the choroid in optical coherence tomography. *Translational Vision Science & Technology*, 12(11):27–27, 2023.
- [19] Juan Xu, Hiroshi Ishikawa, Gadi Wollstein, and Joel S Schuman. Retinal vessel segmentation on slo image. In 2008 30th Annual International Conference of the IEEE Engineering in Medicine and Biology Society, pages 2258–2261. IEEE, 2008.
- [20] Enrico Pellegrini, Gavin Robertson, Emanuele Trucco, Tom J MacGillivray, Carmen Lupascu, Jano van Hemert, Michelle C Williams, David E Newby, Edwin JR van Beek, and Graeme Houston. Blood vessel segmentation and width estimation in ultra-wide field scanning laser ophthalmoscopy. Biomedical optics express, 5(12):4329–4337, 2014.
- [21] Robert Kromer, Rahman Shafin, Sebastian Boelefahr, and Maren Klemm. An automated approach for localizing retinal blood vessels in confocal scanning laser ophthalmoscopy fundus images. *Journal of medical and biological engineering*, 36:485–494, 2016.
- [22] Maria Ines Meyer, Pedro Costa, Adrian Galdran, Ana Maria Mendonça, and Aurélio Campilho. A deep neural network for vessel segmentation of scanning laser ophthalmoscopy images. In *Image Analysis and Recognition: 14th International Conference, ICIAR 2017, Montreal, QC, Canada, July 5–7, 2017, Proceedings 14*, pages 507–515. Springer, 2017.
- [23] Adam Threlfall, Samuel Gibbon, James Cameron, and Tom MacGillivray. A publicly available vessel segmentation algorithm for slo images. *arXiv preprint arXiv:2311.17525*, 2023.
- [24] Sarah Patterson. Oct-tools. https://github.com/sarastokes/OCT-tools, 2019.
- [25] Alexander Brandt. Oct-marker. https://github.com/ neurodial/OCT-Marker/tree/master, 2018.
- [26] Meng Xuan, Wei Wang, Danli Shi, James Tong, Zhuoting Zhu, Yu Jiang, Zongyuan Ge, Jian Zhang, Gabriella Bulloch, Guankai Peng, et al. A deep learning–based fully automated program for choroidal structure analysis within the region of interest in myopic children. *Translational Vision Science & Technology*, 12(3):22–22, 2023.
- [27] Javier Mazzaferri, Luke Beaton, Gisèle Hounye, Diane N Sayah, and Santiago Costantino. Open-source algorithm for automatic choroid segmentation of oct volume reconstructions. *Scientific reports*, 7(1):42112, 2017.
- [28] Adria Perez-Rovira, T MacGillivray, Emanuele Trucco, KS Chin, K Zutis, C Lupascu, Domenico Tegolo, Andrea

- Giachetti, Peter J Wilson, A Doney, et al. Vampire: Vessel assessment and measurement platform for images of the retina. In 2011 Annual International Conference of the IEEE Engineering in Medicine and Biology Society, pages 3391–3394. IEEE, 2011.
- [29] Yukun Zhou, Siegfried K Wagner, Mark A Chia, An Zhao, Moucheng Xu, Robbert Struyven, Daniel C Alexander, Pearse A Keane, et al. Automorph: automated retinal vascular morphology quantification via a deep learning pipeline. *Translational vision science & technology*, 11(7):12–12, 2022.
- [30] Justin Engelmann, Ana Villaplana-Velasco, Amos Storkey, and Miguel O Bernabeu. Robust and efficient computation of retinal fractal dimension through deep approximation. In *International Workshop on Ophthalmic Medical Image Analysis*, pages 84–93. Springer, 2022.
- [31] Jamie Burke, Samuel Gibbon, Justin Engelmann, Adam Threlfall, Ylenia Giarratano, Charlene Hamid, Stuart King, Ian JC MacCormick, and Tom MacGillivray. Sloctolyzer: Fully automatic analysis toolkit for segmentation and feature extracting in scanning laser ophthalmoscopy images. arXiv preprint arXiv:2406.16466, 2024.
- [32] Neeraj Dhaun. Optical coherence tomography and nephropathy: The octane study. https://clinicaltrials.gov/ ct2/show/NCT02132741, 2014. ClinicalTrials.gov identifier: NCT02132741. Updated November 4, 2022. Accessed May 31st, 2023.
- [33] Diana Moukaddem, Niall Strang, Lyle Gray, Paul McGraw, and Chris Scholes. Comparison of diurnal variations in ocular biometrics and intraocular pressure between hyperopes and non-hyperopes. *Investigative Ophthalmology & Visual Science*, 63(7):1428–F0386, 2022.
- [34] Tariq E Farrah, Dan Pugh, Fiona A Chapman, Emily Godden, Craig Balmforth, Gabriel C Oniscu, David J Webb, Baljean Dhillon, James W Dear, Matthew A Bailey, et al. Choroidal and retinal thinning in chronic kidney disease independently associate with egfr decline and are modifiable with treatment. *Nature Communications*, 14(1):7720, 2023.
- [35] Heidelberg Engineering. SPECTRALIS Product Family User Manual. =, 2022.
- [36] Early Treatment Diabetic Retinopathy Study Research Group et al. Early treatment diabetic retinopathy study design and baseline patient characteristics: Etdrs report number 7. *Ophthalmology*, 98(5):741–756, 1991.
- [37] Kenneth Falconer. Fractal geometry: mathematical foundations and applications. John Wiley & Sons, 2004.
- [38] Michael D Knudtson, Kristine E Lee, Larry D Hubbard, Tien Yin Wong, Ronald Klein, and Barbara EK Klein. Revised formulas for summarizing retinal vessel diameters. *Current eye research*, 27(3):143–149, 2003.
- [39] Enrico Grisan, Marco Foracchia, and Alfredo Ruggeri. A novel method for the automatic evaluation of retinal vessel tortuosity. In *Proceedings of the 25th Annual International Conference of the IEEE Engineering in Medicine and Biology Society (IEEE Cat. No. 03CH37439)*, volume 1, pages 866–869. IEEE, 2003.
- [40] James R Cameron, Lucia Ballerini, Clare Langan, Claire Warren, Nicholas Denholm, Katie Smart, and Thomas J MacGillivray. Modulation of retinal image vasculature analysis to extend utility and provide secondary value from optical coherence tomography imaging. *Journal of Medical Imaging*, 3(2):020501–020501, 2016.
- [41] Olivier Morelle. Eyepy. https://github.com/MedVisBonn/

- eyepy/tree/master, 2023.
- [42] Mark Graham. Eyepy. https://github.com/marksgraham/ OCT-Converter, 2024.
- [43] Joel S Schuman, James G Fujimoto, Jay Duker, and Hiroshi Ishikawa. *Optical coherence tomography of ocular diseases*. CRC Press, 2024.
- [44] Zaixing Mao, Atsuya Miki, Song Mei, Ying Dong, Kazuichi Maruyama, Ryo Kawasaki, Shinichi Usui, Kenji Matsushita, Kohji Nishida, and Kinpui Chan. Deep learning based noise reduction method for automatic 3d segmentation of the anterior of lamina cribrosa in optical coherence tomography volumetric scans. *Biomedical optics express*, 10(11):5832–5851, 2019
- [45] Paul A. Yushkevich, Joseph Piven, Heather Cody Hazlett, Rachel Gimpel Smith, Sean Ho, James C. Gee, and Guido Gerig. User-guided 3D active contour segmentation of anatomical structures: Significantly improved efficiency and reliability. *Neuroimage*, 31(3):1116–1128, 2006.
- [46] J Martin Bland and DouglasG Altman. Statistical methods for assessing agreement between two methods of clinical measurement. *The lancet*, 327(8476):307–310, 1986.
- [47] Justin Engelmann, Diana Moukaddem, Lucas Gago, Niall Strang, and Miguel O Bernabeu. Applicability of oculomics for individual risk prediction: Repeatability and robustness of retinal fractal dimension using dart and automorph. *Investigative Ophthalmology & Visual Science*, 65(6):10–10, 2024.
- [48] Ranjay Chakraborty, Scott A Read, and Michael J Collins. Diurnal variations in axial length, choroidal thickness, intraocular pressure, and ocular biometrics. *Investigative ophthalmology & visual science*, 52(8):5121–5129, 2011.
- [49] Colin S Tan, Yanling Ouyang, Humberto Ruiz, and Srini-Vas R Sadda. Diurnal variation of choroidal thickness in normal, healthy subjects measured by spectral domain optical coherence tomography. *Investigative ophthalmology & visual science*, 53(1):261–266, 2012.
- [50] Shinichi Usui, Yasushi Ikuno, Masahiro Akiba, Ichiro Maruko, Tetsuju Sekiryu, Kohji Nishida, and Tomohiro Iida. Circadian changes in subfoveal choroidal thickness and the relationship with circulatory factors in healthy subjects. *Investigative ophthalmology & visual science*, 53(4):2300–2307, 2012.
- [51] Takamasa Kinoshita, Yoshinori Mitamura, Kayo Shinomiya, Mariko Egawa, Akiko Iwata, Akiko Fujihara, Yoko Ogushi, Kentaro Semba, Kei Akaiwa, Eisuke Uchino, et al. Diurnal variations in luminal and stromal areas of choroid in normal eyes. *British Journal of Ophthalmology*, 101(3):360–364, 2017.
- [52] Lisa A Ostrin, Ashutosh Jnawali, Andrew Carkeet, and Nimesh B Patel. Twenty-four hour ocular and systemic diurnal rhythms in children. *Ophthalmic and Physiological Optics*, 39(5):358–369, 2019.
- [53] Waheeda Rahman, Fred Kuanfu Chen, Jonathan Yeoh, Praveen Patel, Adnan Tufail, and Lyndon Da Cruz. Repeatability of manual subfoveal choroidal thickness measurements in healthy subjects using the technique of enhanced depth imaging optical coherence tomography. *In*vestigative ophthalmology & visual science, 52(5):2267–2271, 2011.
- [54] Feiyan Ma, Yifan Bai, Jialiang Duan, Yuchen Liang, and Qingli Shang. Validation of reliability, repeatability and consistency of three-dimensional choroidal vascular index. *Scientific Reports*, 14(1):1576, 2024.
- [55] Siegfried Karl Wagner, Fintan Hughes, Mario Cortina-Borja,

- Nikolas Pontikos, Robbert Struyven, Xiaoxuan Liu, Hugh Montgomery, Daniel C Alexander, Eric Topol, Steffen Erhard Petersen, et al. Alzeye: longitudinal record-level linkage of ophthalmic imaging and hospital admissions of 353 157 patients in london, uk. *BMJ open*, 12(3):e058552, 2022.
- [56] Thomas Pearson, Yingdi Chen, Baljean Dhillon, Sid-dharthan Chandran, Jano van Hemert, and Tom MacGillivray. Multi-modal retinal scanning to measure retinal thickness and peripheral blood vessels in multiple sclerosis. *Scientific Reports*, 12(1):20472, 2022.
- [57] Craig W Ritchie and Karen Ritchie. The prevent study: a prospective cohort study to identify mid-life biomarkers of late-onset alzheimer's disease. BMJ open, 2(6):e001893, 2012.
- [58] Craig W Ritchie, Katie Wells, and Karen Ritchie. The prevent research programme—a novel research programme to identify and manage midlife risk for dementia: the conceptual framework. *International Review of Psychiatry*, 25(6):748–754, 2013.
- [59] Ali Hatamizadeh, Hamid Hosseini, Niraj Patel, Jinseo Choi, Cameron C Pole, Cory M Hoeferlin, Steven D Schwartz, and Demetri Terzopoulos. Ravir: A dataset and methodology for the semantic segmentation and quantitative analysis of retinal arteries and veins in infrared reflectance imaging. IEEE Journal of Biomedical and Health Informatics, 26(7):3272–3283, 2022.
- [60] Yingdi Chen, Juan Larraz, Michael Wong, Patrick Kearns, Fraser Brown, Sarah-Jane Martin, Peter Connick, Niall Mac-Dougall, Christine Weaver, Baljean Dhillon, et al. Longitudinal retinal imaging study of newly diagnosed relapsingremitting multiple sclerosis in scottish population: baseline and 12 months follow-up profile of futurems retinal imaging cohort. BMJ Open Ophthalmology, 7(1):e001024, 2022.
- [61] Patrick KA Kearns, Sarah J Martin, Jessie Chang, Rozanna Meijboom, Elizabeth N York, Yingdi Chen, Christine Weaver, Amy Stenson, Katarzyna Hafezi, Stacey Thomson, et al. Futurems cohort profile: a scottish multicentre inception cohort study of relapsing-remitting multiple sclerosis. BMJ open, 12(6):e058506, 2022.

Supplementary Material

Simultaneous OCT + SLO capture during acquisition

Supplementary Fig. S1 shows a screenshot from the Heidelberg Eye Explorer (HEYEX) software (version 1.12.1.0) (Heidelberg Engineering, Heidelberg, Germany) of an OCT volume for an individual's eye. During OCT capture, the SLO image (left) is used to reference the location of the B-scans (right) captured during acquisition.

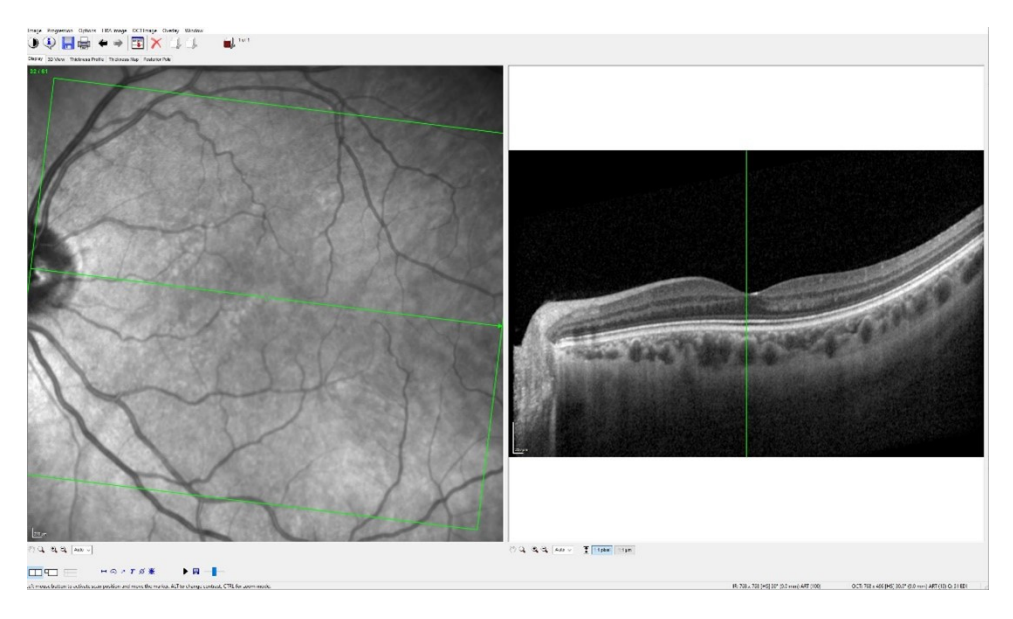


Figure S1 Screenshot from HEYEX viewer of an OCT volume during acquisition. (Left) the SLO image with the acquisition location of the OCT volume overlaid in green, with the green central line indicating the location of the cross-sectional OCT B-scan. (Right) the corresponding fovea-centred OCT B-scan of the OCT volume.

Population tables for OCTolyzer's segmentation models

OCT Segmentation The following datasets were used for OCT choroid segmentation: OCTANE³², a longitudinal cohort of kidney donors and transplant recipients (47 eyes). Diurnal Variation for Chronic Kidney Disease (DVCKD)³², a cohort of young healthy adults collected to assess diurnal variation of the choroid in Edinburgh (20 eyes). Normative, a collection of OCT data from healthy subjects (author J.B. and a healthy cohort collected for a study related to multiple sclerosis⁵⁶) (60 eyes). i-Test³², a cross-sectional cohort of women undergoing normative, pre-eclamptic or intra-uterine growth restrictive pregnancy (42 eyes). PREVENT Dementia, a cohort of mid-life individuals, half of whom are at genetic risk of developing later life dementia^{57;58} (232 eyes). GCU Topcon, a longitudinal cohort of young, healthy participants with varying degrees of myopia collected for assessing diurnal variation of the choroid in Glasgow (43 eyes).

For DeepGPET's model construction ¹⁸ only the OCTANE, Normative and a subset of the i-Test data (10 eyes, 5 participants) were used. More details can be found in the original papers describing the methods ^{18;17}.

	OCTANE ³²	Diurnal Variation 32	Normative	i-Test ³²	Prevent Dementia 57	GCU Topcon 33	Total
Subjects	46	20	1	21	121	24	233
Control/Case	0 / 46	20 / 0	1/0	11 / 10	56 / 65	24 / 0	112 / 121
Male/Female	24 / 22	11 / 9	1/0	0 / 21	66 / 55	14 / 9	116 / 116
Right/Left eyes	46 / 0	20 / 0	1 / 1	21 / 21	117 / 115	22 / 21	227 / 158
Age (mean (SD))	47.5 (12.3)	21.4 (2.3)	23.0 (0.0)	32.8 (5.4)	50.8 (5.6)	21.8 (7.9)	42.9 (13.7)
Device manufacturer	Heidelberg	Heidelberg	Heidelberg	Heidelberg	Heidelberg	Topcon	All
Device type	Standard	Standard	FLEX	FLEX	Standard	DRI Triton Plus	All
nEDI / EDI	EDI	EDI	Both	EDI	Both		
Average ART	100	100	9	50	100		
Scan location							
Horizontal/Vertical	168 / 0	55 / 50	4 / 4	76 / 76	381 / 369	132 / 139	816 / 638
Volume/Radial/Peripapillary	0/0/0	0 / 0 / 66	365 / 0 / 0	2,408 / 0 / 0	0/0/0	0 / 1,307 / 0	2,773 / 1,307 / 66
Total B-scans	168	171	373	2,560	750	1,578	5,600

Table S1 Image characteristics of the cohorts used for building Choroidalyzer ¹⁷.

	OCTANE	i-Test	Normative	Total
Subjects	47	5	30	82
Male/Female	24 / 23	0 / 5	20 / 10	44 / 38
Right/Left eyes	47 / 0	5 / 5	29 / 29	81 / 34
Age (mean (SD))	48.8 (12.9)	34.4 (3.4)	49.1 (7.0)	48.0 (11.2)
HRA+OCT Module	Standard	FLEX	Standard	Both
Horizontal/Vertical scans	166 / 0	16 / 16	57 / 54	239 / 70
Volume scans	174	186	46	406
Total B-scans	340	218	157	715

Table S2 Image characteristics of the cohorts used for building DeepGPET ¹⁸.

SLO Segmentation The following datasets were used for SLO segmentation: RAVIR ⁵⁹, an open source dataset of SLO images with varying degrees of retinal pathology. Normative ⁴⁰, a small dataset of SLO images collected in-house. SLO images captured from the PREVENT Dementia ^{57;58} and i-Test ³² cohorts were also used (285 eyes and 186 eyes, respectively) and were described qualitatively above. FutureMS ^{60;61}, a cohort of individuals with newly diagnosed relapsing-remitting multiple sclerosis (MS) (15 eyes). More details can be found here ³¹.

Study	Participants	Images	Right eyes	Retinal pathology	HRA+OCT Module	Image resolution	Location
RAVIR ⁵⁹	23	23	14	Yes	Standard	768	Disc
Healthy 40	7	7	7	No	Standard	1536	Disc
PREVENT ^{57;58}	144	285	142	No	Standard	1536	Disc
i-Test ³²	93	186	93	No	Standard & FLEX	768	Macula
FutureMS 61;60	15	15	9	No	Standard	1536	Disc

Table S3 Image characteristics of the cohorts used to build SLOctolyzer's segmentation module ³¹.

SLO segmentation model	Cohort					Total
	RAVIR ⁵⁹	Healthy 40	PREVENT 57;58	i-Test ³²	FutureMS ^{60;61}	. 101111
All-vessel segmentation	23	7	Х	X	X	30
Fovea detection	23	7	285	186	15	516
Artery, Vein, Optic disc detection	X	X	×	15	15	30

Table S4 Number of eyes (images) used for each segmentation model stratified by cohort. AVOD, artery-vein-optic disc.

DeepGPET's robustness to peripapillary choroids

Supplementary Fig. S2 shows successful choroid segmentations after application of DeepGPET¹⁸, a model which was trained only on macula-centred OCT B-scans. The choroids were selected to show DeepGPET's robustness to image quality, choroid size and extent of sinuosity for different peripapillary OCT B-scan. The peripapillary choroids shown here were sourced from the DVCKD cohort³².

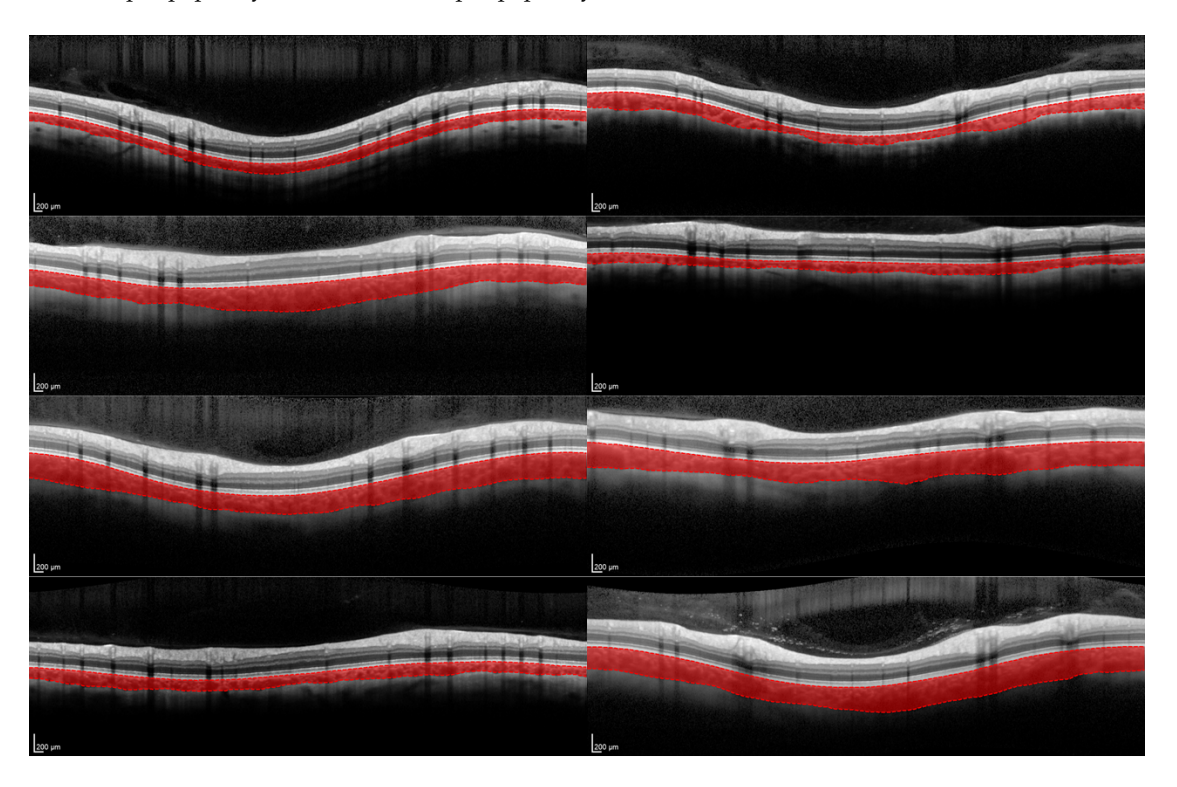


Figure S2 A selection of peripapillary choroids from 8 different eyes from the DVCKD cohort 32 , with successful choroid segmentation after application of DeepGPET 18 .

Layer definition

Supplementary Table \$5 defines the different layers of the retina and choroid which OCTolyzer is capable of making measurements on for the three OCT data types which OCTolyzer supports.

Abbreviation	Layer
ILM – RNFL	Retinal Nerve Fiber Layer
RNFL – GCL	Ganglion Cell Layer
GCL – IPL	Inner Plexiform Layer
IPL – INL	Inner Nuclear Layer
INL – OPL	Outer Plexiform Layer
OPL – ELM	External Limiting Membrane
ELM – PR1	Photoreceptor Layer 1
PR1 – PR2	Photoreceptor Layer 2
PR2 – RPE	Retinal Pigment Epithelium
RPE – BM	Bruch's Membrane Complex
ILM – ELM	Inner retinal layers
ELM – BM	Outer retinal layers
ILM – BM	All retinal layers
BM – CHOR	Choroid

Table S5 All available layers which OCTolyzer measures. ILM, inner limiting membrane.

Detailed thickness map diagram

Supplementary Fig. S3 shows a detailed diagram of how the thickness maps are generated from the segmentations of an OCT volume. The full, detailed pipeline is described below.

All valid thicknesses are measured for each B-scan (panel B, multicoloured), and each B-scans' thickness array is aligned with the fovea from the localiser SLO (panel B, red dotted lines). thickness array alignment per B-scan is required since the anatomical layer segmentations (panel C, black) do not necessarily cover the lateral width of the acquisition region of interest (panel C, black-on-green).

The aligned thickness arrays then follow this step-by-step process (panel D): the coarse thickness map is generated for each B-scan by vertically stacking the aligned thickness arrays. This is padded horizontally by duplicating the edge values. This is then interpolated to the same pixel resolution as the SLO localiser using bi-linear interpolation. A Gaussian filter whose standard deviation is the pixel distance between the parallel, OCT B-scans is used for smoothing. This is then vertically padded to centre the map onto the fovea of the localiser SLO, and the thickness values outside of the ends the original B-scan segmentations are set to 0 (panel C, black). Finally, this map is rotated to the angle of elevation of the original region of interest (panel C, green).

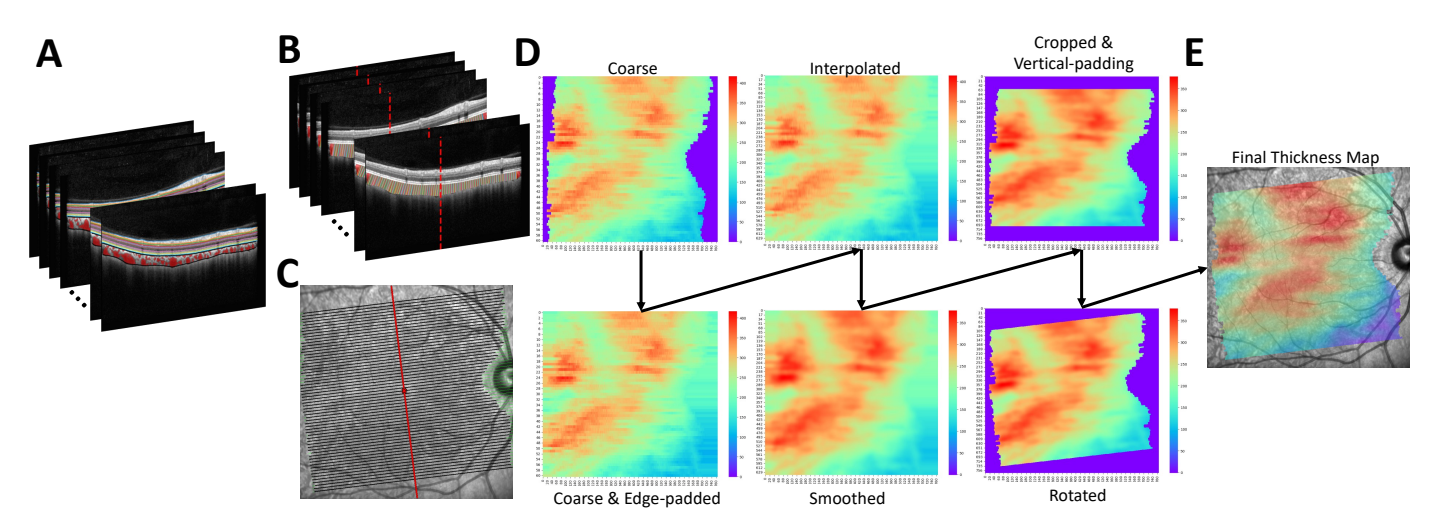


Figure S3 Detailed diagram of how thickness maps are generated, using the choroidal layer as an example. (A) OCT volume of sequential B-scans, with retinal and choroidal layer segmentations overlaid. (B) Valid thickness measurements taken of the choroid across each layer segmentation in every OCT B-scan (C) SLO image with lines of acquisition for each B-scan (green), with the distance the layer segmentation reached per B-scan (black), with the horizontal position on the B-scan of the fovea overlaid as a red line. (D) Step-by-step process of generating the thickness map. (E) The final choroid thickness map overlaid onto the SLO image.

Overlap index demonstration

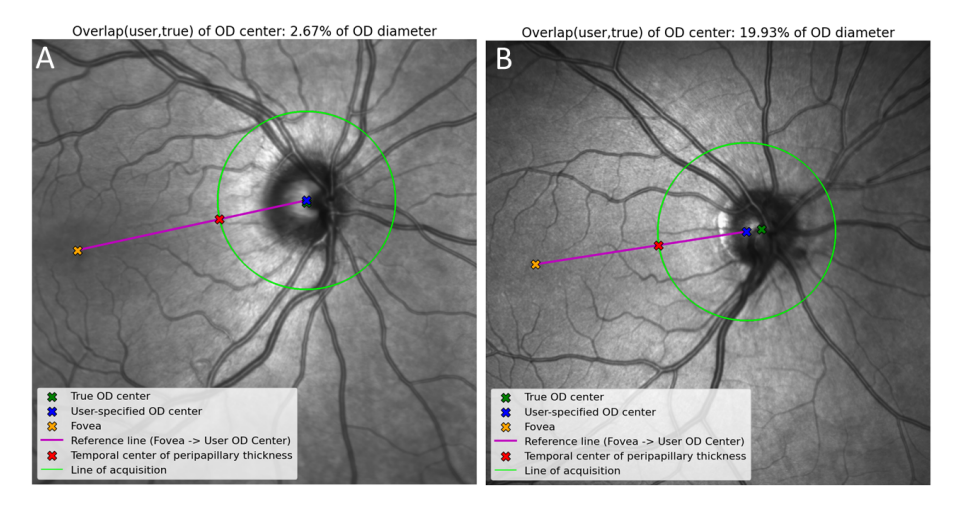


Figure S4 Overlap index measured and visualised for two OCT peripapillary scans. The images are (optionally) saved out during processing of an OCT peripapillary B-scan to visualise the overlap, as well as the alignment of the thickness profiles to the orientation of the fovea and optic disc centre. (A) An example where the overlap index is within the 15% threshold, where the blue cross (the centre of the acquisition's B-scan) and green cross (the centre of the optic disc, measured with the SLO analysis suite), are within 3% of the optic disc diameter. (B) an example where the overlap index exceeds the 15% threshold. Here, the acquisition line-scan is clearly off-centre from the centre of the optic disc. OD, optic disc.

Metadata output from OCTolyzer

Key	Description
Filename	Filname of the SLO+OCT file analyse.
FAILED	Boolean flag on whether file unexpectably failed to be analysed.
eye	Type of eye, either Right or Left.
Bscan_type	Type of OCT scan acquired. One of H(orizontal)-line, V(ertical)-line; A(rtery)V(ein)-line, P(osterior)pole and Peripapillary.
Bscan_resolution_x	Number of columns of B-scan, typically 768 or 1536 for Heidelberg.
Bscan_resolution_y	Number of rows of B-scan, typically 768 or 496 for Heidelberg.
Bscan_scale_z	Micron distance between successive B-scans in a Posterior pole acquisition. Is 0 for all other Bscan_types.
Bscan_scale_x	Pixel lengthscale in the horizontal direction B-scan/SLO, measured in microns per pixel.
Bscan_scale_y	Pixel lengthscale in the vertical direction in the B-scan, measured in microns per pixel.
scale_units	Units of the lengthscales, this is fixed as microns per pixel.
avg_quality	Heidelberg-provided signal-to-noise ratio of the B-scan(s).
retinal_layers_N	Number of retinal layer segmentations extracted from metadata.
scan_focus	Scan focus of the acquisition, in Dioptres. This decides the scaling and is a gross measure of refractive error.
visit_date	Date of acquisition.
exam_time	Time of acquisition.
slo_resolution_px	Number of rows/columns in the square-shaped SLO image (typically 768 or 1536).
field_of_view_mm	Field of view captured during acquisition, usually between 8 and 9 mm if field size is 30 degrees.
slo_scale_xy	Pixel lengthscale of the SLO image, and is typically the same for both directions.
location	Whether scan is macula-centred or disc-centred. Is either "macular" or "peripapillary"
field_size_degrees	Field of view in degrees, typically 30.
slo_modality	Modality used for SLO image capture.
acquisition_angle_degrees	Angle of elevation from horizontal image axis of acquisition for Posterior pole scans.
Bscan_fovea_x	Horizontal pixel position of the fovea on the OCT B-scan (if visible in one of the scans, only relevant for macular OCT).
Bscan_fovea_y	Vertical pixel position of the fovea on the OCT B-scan (if visible in one of the scans, only relevant for macular OCT).
slo_fovea_x	Horizontal pixel position of the fovea on the SLO image, if visible.
slo_fovea_y	Vertical pixel position of the fovea on the SLO image, if visible.
slo_missing_fovea	Boolean value flagging whether fovea is missing from data (either due to acquisition or segmentation failure).
optic_disc_overlap_index_%	% of the optic disc diameter, defining how off-centre a peripapillary image acquisition is from the optic disc centre.
optic_disc_overlap_warning	Boolean value, flagging if the overlap index is greater than 15%, the empirical cut-off to warn end-user of an off-centre scan.
optic_disc_x	Horizontal pixel position of the optic disc centre on the SLO image, if visible.
optic_disc_y	Vertical pixel position of the optic disc centre on the SLO image, if visible.
optic_disc_radius_px	Pixel radius of the optic disc.
thickness_units	Units of measurement for thickness, always in μ m (microns).
vascular_index_units	Units of measurement for choroid vascular index, always dimensionless (no units, but is a ratio between 0 and 1).
vessel_density_units	Units of measurement for choroid vessel density, always in μ m ² (square microns).
area_units	Units of measurements for area, always in mm ² (square millimetres).
volume_units	Units of measurements for volume, always in mm ³ (cubic millimetres).
linescan_area_ROI_microns	For single-line, macular OCT, this is the micron distance defining the fovea-centred region of interest.
choroid_measure_type	Whether the choroid is measured column-wise (per A-scan) or perpendicularly. Always per A-scan for peripapillary OCT.
acquisition_radius_px	Pixel radius of the acquisition line around the optic disc for peripapillary OCT.
acquisition_radius_mm	Millimetre radius of the acquisition line around the optic disc for peripapillary OCT.
acquisition_optic_disc_center_x	Horizontal pixel position of the optic disc centre, as selected by the user during peripapillary OCT acquisition.
acquisition_optic_disc_center_y	Vertical pixel position of the optic disc centre, as selected by the user during peripapillary OCT acquisition.

Table S6 Metadata extracted and inferred using OCTolyzer when processing a ".vol" RAW export file from a Heidelberg Engineering imaging device.

OCTolyzer's interface

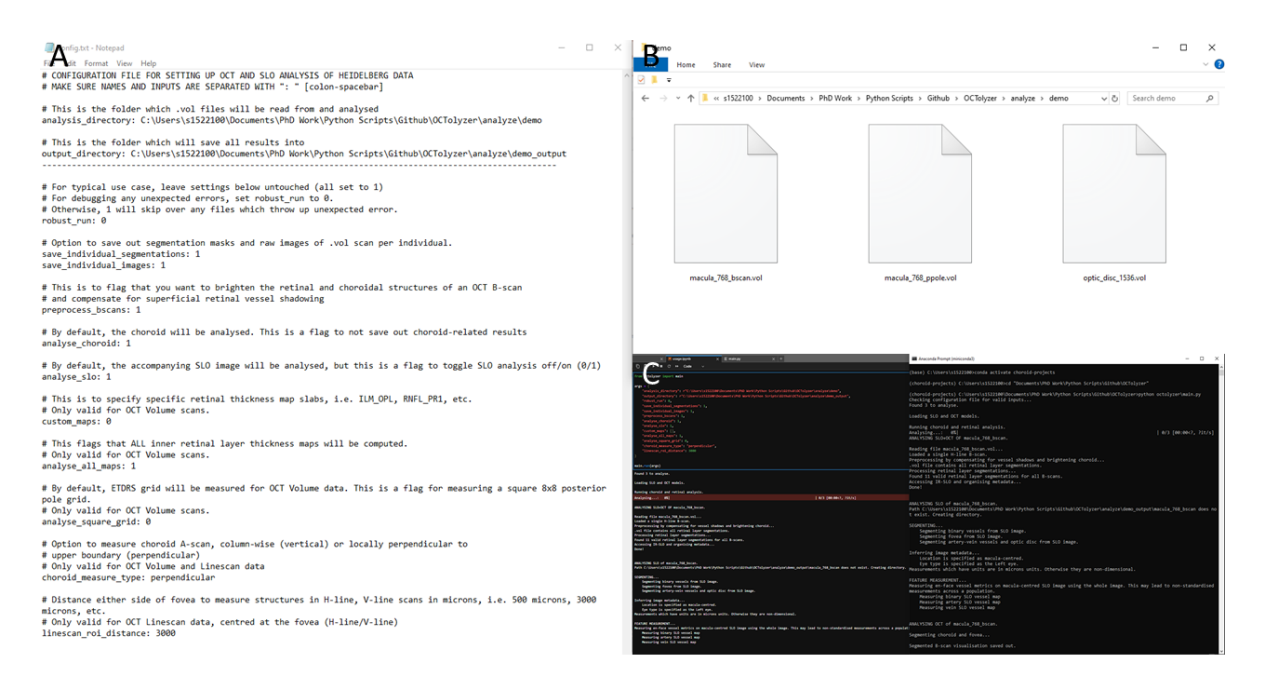


Figure S5 Demonstration of setting up and running OCTolyzer on a batch of demonstrative data. (A) configuration file with user-specified inputs. (B) The folder storing the files (all ".vol" in this example) to be analysed. (C) Running OCTolyzer on a batch of data can be done from a python integrated development environment (left) or via the terminal (right).

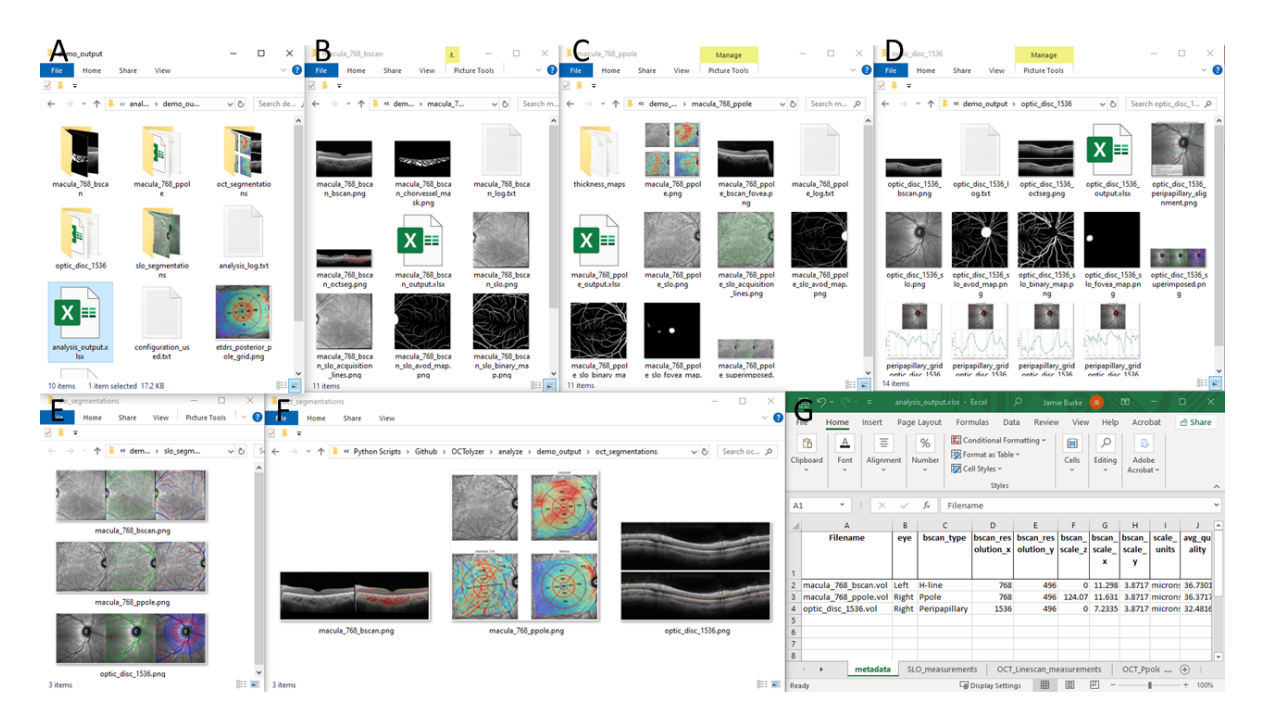


Figure S6 Output files and folders from running OCTolyzer on a batch of three files (all ".vol" in this example), each a different OCT data type which is supported. (A) The folder storing all outputs from batch processing, including folders with results for each individually processed file, a process log, the configuration used and summary measurement and metadata output. (B – D) Exemplar output for each of the OCT data types which OCTolyzer supports: single macular B-scan, macular volume and peripapillary B-scan. (E – F) Composite segmentations of the SLO and OCT segmentation masks for real-time segmentation quality inspection. (G) Summary output file storing key metadata and measurements from OCTolyzer's measurement module for the SLO and OCT data.